Radio Frequency Gradient High Resolution Nuclear Magnetic Resonance Spectroscopy

by

Yang Zhang

M.S., Biomedical Engineering
University of Texas Southwestern Medical Center at Dallas, 1992

Submitted to the Department of Nuclear Engineering in Partial Fulfillment of
the Requirements for the Degree of

Doctor of Philosophy in Nuclear Engineering

at the

Massachusetts Institute of Technology

February 1996

Signature of Author_____
Department of Nuclear Engineering

Certified by_____
David Cory, Assistant Professor of Department of Nuclear Engineering
Thesis Advisor

Certified by_____
Gorden Brownell, Professor of Department of Nuclear Engineering

Accepted by_____
Jeffrey P. Freidberg, Chairman, Graduate Student Committee

Radio Frequency Gradient High Resolution Nuclear Magnetic Resonance Spectroscopy

by

Yang Zhang

Submitted to the Department of Nuclear Engineering on January 5, 1996 in partial fulfillment of the requirements for the Degree of Doctor of Philosophy in Nuclear Engineering

ABSTRACT

Gradient enhanced high resolution NMR has become a standard method in recent years, where B_0 gradients are employed to increase the selectivity of conventional magnetic resonance methods. Radio frequency gradient methods permit greater flexibility in experiment design, and this thesis is concerned with developing the necessary theoretical background for understanding and developing RF gradient experiments. The reason of the complexity of the analysis of the RF gradient experiments is that RF gradient pulse itself can have two effects simultaneously, one of which is coherence transfer and the other is generation of gradient-induced phase evolution. The normal product operator formalism doesn't separate these in a clear, intuitive analysis. In this thesis, a requantization methodology is developed to cleanly separate the two processes. The new methodology is applied to generate properties of RF gradient multiple quantum filters, and to design such filters for the maximum sensitivity. RF gradient multiple quantum spectra experiments were also developed. In a second part of the thesis, spatial square wave modulation via B_0 gradient NMR experiments was explored as a means of achieving the maximum sensitivity through spatial modulation of the spins such that spins at all spatial locations contribute uniformly to the NMR signal during the detection period.

Thesis Supervisor: Dr. David Cory
Title: Professor of Nuclear Engieering Department

Contents

Chapter One:

Introduction to RF gradient method and product operator formalism

§1.1 Introduction to RF gradient Methods

In many nuclear magnetic resonance (NMR) experiments, the signal of interest constitutes only a small portion of the overall spin magnetization and one wishes to limit the detected signal to just those spin coherences that follow a prescribed pathway. The selection of the desired coherence has been traditionally achieved by adding the results of multiple experiments in which the phase of one or more radio frequency (RF) pulses is shifted.

Magnetic field gradients can impose a spatially dependent phase shift on a spin coherence, where the rate of phase accumulation depends linearly on the coherence number of the coherence. This in turn allows a spatial modulation of certain coherence pathways. Provided that the strength of the gradient, $\frac{dB_0}{dr}$, is sufficiently large, the magnetization dispersion due to phase shifts acquired by coherences located in different parts of the sample can render a coherence unobservable in a time short compared to any relaxation time. A suitable combination of magnetic field gradients and coherence transformations then enables the selection of a specific coherence pathway in a single experiment[1.1-1.3].

A wide range of robust methods have been introduced for coherence selection involving combinations of B_0 gradient (DC gradients) and RF pulses. RF gradients, however, have a special attraction for coherence pathway selection since the dephasing properties of the RF gradients are dependent on the phase of the RF field, and since the gradient fields can themselves introduce coherence transformations. In addition, RF gradients can be used to suppress the evolution of internal Hamiltonians so that the spin dynamics are

simplified. RF gradients also have favorable relaxation properties in that the relaxation during the gradient is determined by a combination of T_1 and T_2, whereas the relaxation during a B_0 gradient is determined solely by T_2.

Radio frequency gradients or B_1 gradients have been employed in most of the commonly used homonuclear and heteronuclear NMR experiments. Applications of RF gradients in homonuclear experiments include solvent suppression techniques[1.4-1.6], P/N-type selection in COSY experiments [1.7-1.9], multiple quantum filters[1.10-1.13] and the suppression of zero quantum coherence in correlation experiments[1.14-1.17]. In proton detected heteronuclear correlation spectroscopy, RF gradients have been used to suppress the signals from uncoupled protons[1.18-1.20]. Despite the wealth of applications RF gradient methods are still complex to discuss, since the steps of coherence transformation and gradient evolution, that are separate in the case of B_0 gradients, occur simultaneously. This results in a too complex picture of the spin dynamics that is often solved by brute force integration of the spin response over the sample. In contrast a B_0 gradient cannot induce coherence transformations and B_0 gradient experiments can be conveniently analyzed using the concept of coherence orders [1.1, 1.3, 1.21].

In this thesis, we present a general formalism for discussing RF gradient experiments in which the steps of coherence transformation and gradient evolution are clearly separated. This formalism is applied to the general discussion of homonuclear multiple-quantum filters and multiple quantum coherence experiments. To facilitate the understanding of the methodology and the experiment, a brief introduction of the nuclear spin, density matrix formalism and product operators formalism is presented.

§1.2 Spin, Magnetization, and NMR Signal Sensitivity

For a spin=1/2 system, such as ^1H, ^{13}C, ^{15}N, ^{19}F, there are only two eigenstates, $|1/2\rangle$ and $|-1/2\rangle$, corresponding to spin up and spin down

relative to the external magnetic field direction. When a material of spin=1/2 system is placed into a strong static magnetic field, as a result of the interaction of spins and the magnetic field, the spins distribute into the two states according to Boltzmann statistics,

$$\frac{N_-}{N_+} = \frac{\exp(\frac{-h\omega_0}{4\pi kt})}{\exp(\frac{h\omega_0}{4\pi kt})} = \exp(\frac{-h\omega_0}{2\pi kt}) \quad ,$$

where,

N_- and N_+ : number of spins anti-parallel or parallel to the external magnetic field.

h : Planck's constant.

k : Boltzmann's constant.

$\omega_0 = \gamma B_0$: the Lamor frequency.

The difference in population of the spin $|1/2\rangle$ and $|-1/2\rangle$ states results in a bulk magnetization, called the Curie magnetization, of,

$$M = N_0 \frac{h}{2\pi} \gamma I_z \frac{N_+ - N_-}{N_+ + N_-} \quad ,$$

where,

N_0 density of the spins,

$\frac{h}{2\pi} \gamma I_z$: magnetic moment of an individual spin,

$\frac{N_+ - N_-}{N_+ + N_-}$: Statistical fraction of excess spins.

Such magnetization can be studied with Pulsed Fourier NMR experiments. In particular, such magnetization is the source of the NMR signal in the RF coil and is relevant to the signal sensitivity that will be mentioned in the later chapters.

§1.3 Density Matrix

NMR is a powerful tool to characterize the nuclear spin network topologies and spin dynamics. A full description of the spin dynamics requires knowledge of the spin Hamiltonians and a density matrix approach. However, in a wide range of NMR experiments, the spins are only weakly coupled, and as we will see, the density matrix methodology reduces to a simple product operator's formalism. First, we will introduce the density matrix methodology.

Any given state of a spin system can be expressed as a linear combination of the eigenstates,

$$\psi = \sum_n c_n |\varphi_n\rangle .$$

The evolution of this state is described by the Schrödinger equation,

$$\frac{\partial \psi}{\partial t} = -i H \psi \quad ,$$

where we have suppressed $\hbar$. We will set $\hbar$=1 in all the following discussions, and give energies in frequency units.

Let's look at the time dependent of the z-component of the magnetic moment for an ensemble of spins,

$$M_z = N_0 \langle \overline{\mu_z} \rangle = N_0 \gamma \langle \overline{\psi | I_z | \psi} \rangle = N_0 \gamma \sum_n \sum_m \overline{c_n c_m^*} \langle \varphi_n | I_z | \varphi_m \rangle \quad ,$$

where N_0 is the density of the spins. M_z is the macroscopic magnetization, $\langle \mu_z \rangle$ is the microscopic magnetization, and γ is the gyromagnetic ratio. I_z and $|\varphi_n\rangle$ can be chosen such that they are time-independent and constant throughout the ensemble of spins. The bar over the variables indicates an ensemble average. From the above formula, there are two observations,

(1). Since I_z and $|\varphi_n\rangle$ are constant over the ensemble, the ensemble average is actually over the coefficient c_n .

(2). Since I_z and $|\varphi_n\rangle$ are time independent, the time dependence is contained within the coefficient c_n.

The result is that $\overline{c_n c_m^*}$ contains all the information about the dynamics of the spin system. The density matrix is made up of the component of $\overline{c_n c_m^*}$.

First, look at the time evolution of each individual coefficient c_n. From the time-dependent Schrödinger equation,

$$\frac{\partial|\psi\rangle}{\partial t} = -i\, H\, |\psi\rangle ,$$

and the time-independent Schrödinger equation,

$$H|\varphi_n\rangle = E_n\, |\varphi_n\rangle ,$$

$$\sum_n \frac{\partial c_n}{\partial t}|\varphi_n\rangle = -i \sum_n c_n E_n\, |\varphi_n\rangle \ .$$

Since the eigenstates are orthogonal, we may collect terms to see,

$$\sum_n \left(\frac{\partial c_n}{\partial t} + i\, c_n E_n\right)|\varphi_n\rangle = 0 \ .$$

Since all of the eigenstates are orthogonal, and none zero, that the linear combination of eigenstates is zero implies that,

$$\frac{\partial c_n}{\partial t} + i\, c_n E_n = 0 \ ,$$

for any n. The solution for this differential equation is,

$$c_n(t) = c_n(0)\, \exp(-\, i\, E_n\, t) \ .$$

To fully describe the spin system, all components of the spin operator (I_x, I_y, I_z) must be considered.

Now, with the help of the bra-ket notation, the time evolution of the density operator can be derived. The spin state is a linear combination of the eigenstates,

$$\psi = \sum_n c_n \, | \varphi_n \rangle \ .$$

The evolution of the spin state is governed by the time-dependent Schrödinger Equation, in ket form,

$$\frac{\partial |\psi\rangle}{\partial t} = -i \, H \, |\psi\rangle \ ,$$

or, in bra form,

$$\frac{\partial \langle\psi|}{\partial t} = i \, \langle\psi| H \ .$$

The bra-ket is the orthogonal and normalized, i.e.

$$\langle\varphi_m|\varphi_m\rangle = 1 \ ,$$

and

$$\langle\varphi_n|\varphi_m\rangle = 0 \ .$$

With the help of the projection operator, $|\psi\rangle\langle\psi|$, we note that,

$$\langle\varphi_n|\psi\rangle\langle\psi|\varphi_m\rangle = \langle\varphi_n| \left(\sum_k c_k|\varphi_k\rangle\right) \left(\sum_j c_j\langle\varphi_j|\right) |\varphi_m\rangle = c_n c_m^* \ ,$$

So, the density matrix ρ is simply,

$$\rho = |\psi\rangle\langle\psi| \ .$$

The time evolution of the density operator is then described by the following,

$$\frac{\partial \rho}{\partial t} = \frac{\partial |\psi\rangle\langle\psi|}{\partial t} = \frac{\partial |\psi\rangle}{\partial t}\langle\psi| + |\psi\rangle\frac{\partial \langle\psi|}{\partial t}$$
$$= -i\, H\, |\psi\rangle\langle\psi| + i\, |\psi\rangle\langle\psi|\, H$$
$$= -iH\rho + i\rho H$$
$$= -i[H,\rho]$$

This is the time-dependent Schrödinger equation for the density operator. So, one approach to solving for the spin dynamics is to solve the time dependent Schrödinger equation of the density operator. In the above equation, H is the interaction Hamiltonian. Examples of spin Hamiltonians that will be important in this work are the Zeeman Hamiltonian, the chemical shift Hamiltonian, and the scalar coupling Hamiltonian. Definitions and further discussions of these Hamiltonians will follow after we explain a special case.

Now, consider a spin system at equilibrium, where the Zeeman Hamiltonian is the dominant Hamiltonian,

$$H_z = \gamma B_0 I_z \quad .$$

The evolution of an element of the density matrix is given in the operator form by the Schrödinger equation of the density operator,

$$\frac{\partial \langle n|\rho|m\rangle}{\partial t} = -i \langle n|[H,\rho]|m\rangle$$
$$= -i \langle n|H\rho - \rho H|m\rangle$$
$$= -i(E_n - E_m) \langle n|\rho|m\rangle \quad ,$$

The solution of the above differential equation is,

$$\langle n|\rho(t)|m\rangle = \langle n|\rho(0)|m\rangle \exp(-i(E_n - E_m)t) \quad .$$

When $n \neq m$, $\langle n \,|\, \rho(t) \,|\, m\rangle$ is an off-diagonal element, which oscillates according to the energy difference of the coupled states.

On the other hand, the diagonal elements (n=m),

$$\langle n|\rho(t)|n\rangle = \langle n|\rho(0)|n\rangle \,,$$

are constants of motion under the Zeeman Hamiltonian. This is true since the eigenstates are eigenstates of the Zeeman Hamiltonian.

§1.4 Hamiltonians

Nuclear spins are not well connected to the lattice so that the spin states can be far from equilibrium for a relative long time. Below, we discuss the dominant Hamiltonians that dictate the spin dynamics in high resolution NMR. The Chemical Shift Hamiltonian has the following form,

$$H_z = \gamma B_0(1-\sigma) I_z ,$$

where σ is a magnetic shielding tensor, which quantifies the magnetic shielding effect of the electron cloud surrounding the nucleus spin. In the liquid state, where molecules are rapidly and isotropically tumbling, the shielding tensor can be replaced by its isotropic value. The scalar coupling Hamiltonian has the following form,

$$H_j = J \vec{I} \cdot \vec{S} ,$$

where, J is the scalar coupling constant, and $\vec{I}$ and $\vec{S}$ are spin operators for two distinct spins. If the chemical shift interaction is much larger than the scalar coupling interaction, i.e. ,

$$\omega_{cs} >> J ,$$

where,
ω_{cs} : the chemical shift frequency
J : the coupling constant,

the scalar coupling Hamiltonian may be simplified to the weak coupling case of,

$$H_j = J I_z S_z ,$$

This simplifies the analysis of the spin dynamics, for the eigenstates of the Zeeman Hamiltonian are still good eigenstates of the total Hamiltonian.

The B_0 gradient Hamiltonian, and B_1 gradient Hamiltonian may take many different forms depending on the physical configurations of the gradient coil. Here are only one example of them. The typical B_0 gradient Hamiltonian used in spectroscopy is a linear gradient along the z-axis,

$$H_{B_0} = \gamma \frac{\partial B_0}{\partial z} z\, I_z \quad ,$$

where $\frac{\partial B_0}{\partial z}$ is the gradient strength along the z axis.

Similarly, a typical example of a B_1 gradient Hamiltonian is,

$$H_{B_1} = \gamma \left(\frac{\partial B_1}{\partial x} x + \frac{\partial B_1}{\partial y} y\right) I_w \quad ,$$

where I_w is any direction in the rotating plane, which is perpendicular to z, usually, $I_w = I_x$ or I_y.

§1.5 Product Operators

Hilbus, Sorensen, and Slichter each introduced a form of the product operator formalism. Here we follow the literature of Sorensen et. al. [1.22], who expressed the density operator systematically in terms of product operators,

$$\sigma(t) = \sum_s b_s(t)\, B_s \,,$$

&

$$B_s = 2^{(q-1)} \prod_{k=1}^{N} (I_{kv})^{a_{sk}} \quad ,$$

where,
$\sigma(t)$ is density operator,
N = total number of I=1/2 nuclei in the spin system,
k = index of nucleus, v=x, y, or z,
q=number of single-spin operators in the product,
a_{sk}=1 for q nuclei and a_{sk}=0 for the N-q remaining nuclei.

The following description of the product operator is a brief summary of Sorensen's paper [1.11].

Product operators for spin 1/2 nuclei are orthogonal with respect to formation of the trace, however they are not normalized, i.e.,

$$Tr\{B_r B_s\} = \delta_{r,s} 2^{N-2} \quad .$$

The complete base set $\{B_s\}$ for a system with N spins 1/2 consists of 4^N product operators B_s. As an example, we list the complete set of 16 product operators B_s for a two-spin system,

q=0	E/2 (E = unity operator)
q=1	I_{1x}, I_{1y}, I_{1z}, I_{2x}, I_{2y}, I_{2z}
	$2I_{1x}I_{2x}$, $2I_{1x}I_{2y}$, $2I_{1x}I_{2z}$,
	$2I_{1y}I_{2x}$, $2I_{1y}I_{2y}$, $2I_{1y}I_{2z}$,
	$2I_{1z}I_{2x}$, $2I_{1z}I_{2y}$, $2I_{1z}I_{2z}$.

An arbitrary density operator can be expressed as a linear combination of such a set of base operators. This choice of basis set greatly simplifies calculations of pulse experiments applied to weakly coupled systems, because the density of individual operator terms can be followed through out the experiment and can be associated with a clear physical meaning.

The effects of free precession and of RF pulses are described by a sequence of transformations of the type,

$$\exp\{-i\phi B_r\}B_s\exp\{i\phi B_r\} = \sum_t b_{ts}(r,\phi)B_t \quad ,$$

where,
$\phi B_r = (\Omega_k \tau)\, I_{kz}$ for chemical shift precession,
$\phi B_r = (\pi J_{kl} \tau)\, 2I_{kz}I_{lz}$ for the evolution under weak scalar coupling between two spins with I = 1/2,
$\phi B_r = \beta I_{kv}$ for an RF pulse applied to nucleus k with rotation angle β and rotation axis v.

In the context of an N-spin system, we distinguish one-spin, two-spin and generally q-spin product operators. One-spin operators are associated with entire spin multiplets. I_{kz} represents z-magnetization with equal polarization across all transitions of spin k. The transverse operators I_{kx} and I_{ky} are representative of the spin k multiplet with all multiplet components in-phase along the x- or y-axes of the rotating frame. This suggests the following nomenclature,

I_{kz} : longitudinal magnetization of spin k,
I_{kx} : in-phase x-magnetization of spin k,
I_{ky} : in-phase y-magnetization of the spin k.

Two-spin product operators can be classified as follows:

$2I_{kx}I_{lz}$: antiphase x-magnetization of spin k, or more specifically, x-magnetization of spin k antiphase with respect to spin l,
$2I_{ky}I_{lz}$: antiphase y-magnetization of spin k, or more specifically, y-magnetization of spin k antiphase with respect to spin l,
$2I_{1x}I_{2x}$, $2I_{1x}I_{2y}$, $2I_{1y}I_{2x}$, $2I_{1y}I_{2y}$: two-spin coherence of spins k and l.
$2I_{1z}I_{2z}$: longitudinal two-spin order of spins k and l.

Antiphase magnetization represents multiplets with individual components that have opposite phases. For example, $2I_{kx}I_{lz}$ corresponds to a k-spin multiplet with magnetization component along the +x or -x axes of the rotating frame, depending on the polarization of spin l.

First, consider the evolution of the density operator under the unperturbed weak coupling Hamiltonian,

$$H = \sum_k \Omega_k I_{kz} + \sum_k \sum_{l>k} 2\pi J_{kl} I_{kz} I_{lz}$$
$$= \sum_k \Omega_k (I_{kz}) + \sum_k \sum_{l>k} \pi J_{kl} (2 I_{kz} I_{lz}) \quad .$$

Note that the Hamiltonian is written in the terms of the product operator B_s. The chemical shift frequency of nucleus k in the rotating frame is defined by $\Omega_k = \omega_{0k} - \omega_{rf}$, with the Larmor frequency $\omega_{0k} = -\gamma_k(1-\sigma_k)B_0$ and the RF frequency ω_{rf} . In a heteronuclear system, several different RF frequencies and rotating frames must be used.

We consistently define positive rotations in the right-handed sense (clockwise). A positive rotation about the z-axis leads from x to y, to -x to -y. Since all terms in the above weak coupling Hamiltonian commute, the evolution caused by the individual terms can be computed separately in arbitrary order,

$$\sigma(t+\tau) = \prod_k \exp(-i\omega_k \tau I_{kz}) \prod_{k<l} \exp(-i\pi J_{kl} \tau 2 I_{kz} I_{lz}) \sigma(t) \prod_{k<l} \exp(i\pi J_{kl} \tau 2 I_{kz} I_{lz}) \prod_k \exp(i\omega_k \tau I_{kz}),$$

or symbolically,

$$\sigma(t) \xrightarrow{\Omega_1 \tau I_{1z}} \xrightarrow{\Omega_2 \tau I_{2z}} \xrightarrow{\pi J_{12} \tau 2 I_{1z} I_{2z}} \xrightarrow{\pi J_{13} \tau 2 I_{1z} I_{3z}} \ldots \sigma(t+\tau) \quad .$$

Now, we consider the evolution or precession of a spin state under chemical shifts, spin-spin coupling, and RF pulses separately.

First, look at the spin state evolving under the chemical shift Hamiltonian, $\Omega_k I_{kz}$,

$$I_{kx} \xrightarrow{\Omega_k \tau I_{kz}} I_{kx}\cos(\Omega_k \tau) + I_{ky}\sin(\Omega_k \tau) \quad ,$$
$$I_{ky} \xrightarrow{\Omega_k \tau I_{kz}} I_{ky}\cos(\Omega_k \tau) - I_{kx}\sin(\Omega_k \tau) \quad .$$

For product operator representing two-spin coherence, each chemical shift Hamiltonian affects each spin individually and the total effect can be calculated sequentially.

Chemical shift evolution always conserves the number q of operators I_{kv} in each term B_s. An operator with q transverse components (I_{kx},I_{ky}) transforms into a linear combination of the transverse components, while the longitudinal components (I_{kz}) remain invariant.

For a coupling between two nuclei k and l within an arbitrary network of coupled spins I = 1/2, the evolution under the spin-spin coupling Hamiltonian $\pi J_{kl} \tau 2I_{1z}I_{2z}$ is,

$$I_{kx} \xrightarrow{\pi J_{kl}\tau 2I_{kz}I_{lz}} I_{kx}\cos(\pi J_{kl}\tau) + 2I_{ky}I_{lz}\sin(\pi J_{kl}\tau) ,$$
$$I_{ky} \xrightarrow{\pi J_{kl}\tau 2I_{kz}I_{lz}} I_{ky}\cos(\pi J_{kl}\tau) - 2I_{kx}I_{lz}\sin(\pi J_{kl}\tau) .$$

This corresponds to the conversion of in-phase magnetization into orthogonal antiphase magnetization. If we start out with antiphase magnetization, the evolution under the scalar coupling generates in-phase magnetization,

$$I_{kx}I_{lz} \xrightarrow{\pi J_{kl}\tau 2I_{kz}I_{lz}} I_{kx}I_{lz}\cos(\pi J_{kl}\tau) + 2I_{ky}\sin(\pi J_{kl}\tau) ,$$
$$I_{ky}I_{lz} \xrightarrow{\pi J_{kl}\tau 2I_{kz}I_{lz}} I_{ky}I_{lz}\cos(\pi J_{kl}\tau) - 2I_{kx}\sin(\pi J_{kl}\tau) .$$

Now, consider a strong, non-selective RF pulses with,

$$\omega_{rf} >> \omega_{cs} >> J \quad .$$

The effect of pulses with phase v=x or y and flip angle β is represented by the transformation,

$$\sigma(t_+)=\exp(-i\beta\sum_k I_{kv})\sigma(t_-)\exp(i\beta\sum_k I_{kv}) \quad ,$$

where, the summation is carried out over all spins affected by the pulse (possibly restricted to either I or S species in heteronuclear systems). The calculation can be carried out in any arbitrary order,

$$\sigma(t_-) \xrightarrow{\beta I_{kv}} \xrightarrow{\beta I_{lv}} \xrightarrow{\beta I_{mv}} \ldots \sigma(t_+) \quad .$$

The effect of an RF pulse can be considered separately for each single-spin operator I_{kv} in the product operators.

For a rotation about the x-axis,

$$I_{kz} \xrightarrow{\beta I_{kx}} I_{kz}\cos(\beta) - I_{ky}\sin(\beta) \, ,$$
$$I_{ky} \xrightarrow{\beta I_{kx}} I_{ky}\cos(\beta) + I_{kz}\sin(\beta) \, .$$

For a rotation about the y-axis,

$$I_{kz} \xrightarrow{\beta I_{ky}} I_{kz}\cos(\beta) + I_{kx}\sin(\beta) \, ,$$
$$I_{kx} \xrightarrow{\beta I_{ky}} I_{kx}\cos(\beta) - I_{kz}\sin(\beta) \, .$$

With RF phase shifts or pulse sandwiches, it is also possible to create an equivalent z-pulse and achieve the following transformations,

$$I_{kx} \xrightarrow{\beta I_{kz}} I_{kx}\cos(\beta) + I_{ky}\sin(\beta) \, ,$$
$$I_{ky} \xrightarrow{\beta I_{kz}} I_{ky}\cos(\beta) - I_{kx}\sin(\beta) \, .$$

A pulse with arbitrary phase, or with tilted RF field has more complex form and interested reader are referred to Sorensen's original article [1.22].

Density matrices formalism provides a full description of the spin dynamics under any circumstances. Product operator formalism is a complete description of the weakly coupled spin system. In this case,

product operator formalism allows one to gain additional insight into the fundamental aspects of the spin dynamics.

§1.6 Coherence Number and Phase Evolution Under a Gradient

The concept of a coherence number is related to the product operator basis. The essence of the coherence number is to assign to a state of coupled spin system an integer number, which is proportional to the rate of phase evolution of the spin system, in the presence of an inhomogeneous interaction(of which a B_0 gradient field is a special case). the Hamiltonian can be written as,

$$H = \omega I_z.$$

The time evolution of a density operator, ρ, is governed by the time-dependent Schrödinger Equation,

$$\frac{\partial \rho}{\partial t} = -i[H, \rho] \ .$$

The density operator is given by a product of single, raising, and lowering spin operators,

$$\rho = \prod I_j, j = +, -, z \quad .$$

Following the commutator relationships,

$$[I_z, I_+] = I_+ \ ,$$

and

$$[I_z, I_-] = -I_- \ .$$

the solution to the time-dependent Schrödinger Equation is well known,

$$\rho(t) = e^{-i \omega t I_z} \rho(0) e^{i \omega t I_z} \quad .$$

Based on the commutation relations, the above may be rewritten as a phase shift of original state,

$$\rho(t) = e^{-i\,k\,\omega t}\ \rho(0) \quad ,$$

where, the coherence number, k, is determined by expanding the state in terms of the normal raising and lowering operators,

$$I_+ = I_x + i\,I_y \ ,$$

$$I_- = I_x - i\,I_y \quad ,$$

and then counting the number of the coherence (the number of I_+ terms minus the number of I_- terms in the product operator). A p-quantum coherence evolves p times as fast as a single quantum.

The coherence number also describes how rapid a state will be dephased (rather than simply coherently evolving) under a B_0 gradient.

The coherence number of a state is defined with respect to an I_z operator since we are working at high field and all internal Hamiltonians are truncated to that portion that commutes with the Zeeman Hamiltonian. The normal concept of a coherence number is very useful, therefore, when discussing internal Hamiltonians, or when discussing B_0 gradients since these are also secular (i.e., the B_0 gradient Hamiltonian commutes with the Zeeman Hamiltonian). When RF gradients are included, however, the concept of a coherence number is not sufficient to describe of the dynamics of the spin system. During the RF gradient period, coherence transformations and phase accumulation happen at the same time, so that coherence number is no longer characteristic of the dynamics of the spin system. To analyze RF gradient experiments, a new "requantization" concept is introduced in the next chapter which extends the concept of a coherence number to all three axes.

Chapter Two

Requantization Methodology-- A Generalized Approach to the Analysis of RF Gradient Experiments.

§2.1 Magnetic Field Gradient Experiment of Coherence Pathway Selection

Magnetic Field gradients have been shown to be extremely useful for the implementation of multiple-quantum filters. By combining gradients and coherence transformations, a wide range of robust methods have been introduced to select only that portion of the overall spin magnetization that follows a particular coherence transformation pathway. Gradients have the advantage over phase cycling methods of introducing a well characterized and reproducible dephasing mechanism into the experiment where the strength of the gradient ($\frac{dB_0}{dr}$) is sufficiently strong that a coherence can be completely dephased (be made unobservable) in a time short compared to any relaxation time.

§2.2 RF Gradient Experiments of Coherent Pathway Selections

Radio frequency (RF) gradients have a special attraction for coherence pathway selection because the effective coherence number changes with the phase of the RF field, and because the RF fields can themselves introduce coherence transformations. In addition, RF gradients can be used to suppress the evolution of internal Hamiltonians so that the spin dynamics are simplified.

Many of the general aspects of multiple-quantum filtering have been introduced by Counsell et al.[1.10], Canet[1.11, 1.13], and Cory et. al.[1.12]. RF gradient methods are still complex to discuss since the normally separate steps of coherence transformation and gradient evolution occur simultaneously. Even in those cases where the gradient is employed solely for dephasing, the coherence

transformation properties must still be considered since they can lead to unexpected observable magnetization. Here, we present a general formalism for discussing RF gradient experiments in which the steps of coherence transformation and gradient evolution are clearly separated. This formalism is applied to the general discussion of homonuclear multiple-quantum filters, multiple quantum spectrum, and their implementations.

§2.3 Analysis of the RF Gradient Double Quantum Filter

Let's start with an analysis of the RF gradient double quantum filter.

Canet et al. introduced an RF gradient version of double quantum filter, COSY-GR, for obtaining the equivalent of DQF-COSY without phase cycling. Figure 2.1 is the 1-D double quantum filter pulse sequence.

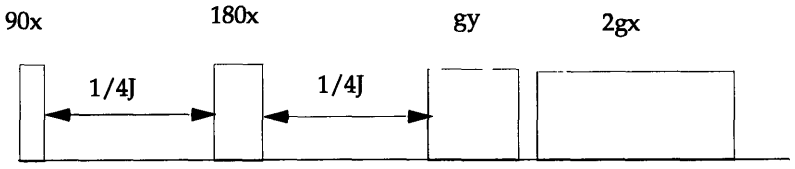

Figure 2.1 1-D double quantum filter pulse sequence

The pulse train, '90°-1/4J-180°-1/4J', excites the spin system and prepares an anti-phased single quantum state, $I_{1x}I_{2z}$. The key part of the RF gradient double quantum filter is the two consecutive RF gradient pulses, gy and 2gx. The two gradients are 90° out of phase from each other. If we define the effective gradient duration as the gradient strength times the duration when the gradient is on, then the effective duration of the second RF gradient is twice that of the first. The first gradient pulse, gy, dephases the desired state, $I_{1x}I_{2z}$ and spin locks the spin state, I_{1y}. The second gradient pulse selectively re-focuses $I_{1x}I_{2z}$ and leaves the other undesired spin states dephased. The spin state, I_{1y}, which was spin-locked by the first gradient is dephased by the second. In the detection period, only the spin state $I_{1x}I_{2z}$ is preserved, and it evolves into observable single quantum signals.

Double quantum filters are very often used to suppress the solvent signal, since only coupled spin systems can generate anti-phased term, $I_{1x}I_{2z}$. All uncoupled spin systems (including solvent) are dephased by one of the two gradient pulses.

The first gradient pulse both dephases the anti-phase spin coherence and introduces a coherence transformation. The second RF pulse re-phases the spin magnetization and leads to a detectable echo signal. Notice that the first gradient pulse, gy, nutates both spin magnetization (I_{1x} and I_{2z}). Hence $I_{1x}I_{2z}$, acts as though it has effective coherence numbers of zero and +/- two under the gradient field, gy. The second gradient pulse, 2gx, nutates only the single magnetization vector I_{2z}, since I_{1x} is spin locked. So $I_{1x}I_{2z}$ acts as though it has effective coherence number of +/-1 under the gradient field, 2gx. So by simply changing the phase of the RF, the effective coherence number is varied without recourse to any coherence transformation pulses.

Notice also that while there has been an effective double quantum filter, the spins actually never passed through a double quantum state, they were always anti-phase. The relaxation properties and the range of coherences that can pass through this filter are therefore different from that associate with B_0 gradient case. Also notice that in a B_0 gradient experiment, while the spins are being dephased by the gradient they are also evolving due to other inhomogeneous interactions, all of which commute with the gradient Hamiltonian. In the RF gradient experiment, the RF nutation is orthogonal to these inhomogeneous interactions, and removes the evolution due to these via second averaging (provided that the RF interaction is stronger than the inhomogeneous interaction).

2.4 Coherence Transformation, Phase Accumulation, & Requantization

It is not always sufficient (particularly in Homonuclear MQF experiments) to dephase a state, rather one needs to dephase and then selectively re-phase a particular coherence pathway. Therefore, in

between the dephasing and re-phasing steps there must be a coherence transformation step that changes the coherence number of the state of interest, and these normally take the form of RF pulses.

In RF gradient spectroscopy, the gradient itself causes both dephasing/re-phasing, and introduces coherence transformations. To have a convenient picture of the dynamics it is useful to separate these two operations.

To follow the dynamics in RF gradient experiments, it is convenient to expand the Cartesian single spin operators into raising and lowering operators that are quantized along I_x and I_y. In this fashion we will consider that when a given RF gradient field is applied (1) the spin system interacts as though it is quantized along the gradient field, and (2) that the gradient interaction is sufficient to remove through second averaging all inhomogeneous interactions.

The requantization that is discussed throughout this work is of course a second quantization in which the spins are quantized along the RF field which is stationary in the normal rotating frame. This second quantization does not reintroduce the Zeeman interaction, since it is still in the rotating frame. As expected, however, the second quantization will modulate inhomogeneous interactions and thereby cause these to be averaged to zero.

A straight forward expansion of the single spin Cartesian operators leads to the set of raising and lowering operators shown in table 2.1.

Table 2.1

z-quantized	x-quantized	y-quantized
$I_z^+ = I_x + i\,I_y$	$I_x^+ = I_y + i\,I_z$	$I_y^+ = I_z + i\,I_x$
$I_z^- = I_x - i\,I_y$	$I_x^- = I_y - i\,I_z$	$I_y^- = I_z - i\,I_x$
$I_z = I_z$	$I_x = I_x$	$I_y = I_y$

Notice that we have introduced a slight modification to the raising and lowering operator nomenclature to explicitly show the axis of quantization.

Given table 2.1, the effective coherence numbers for the full range of two-spin Cartesian product operators can be calculated for the three axes of quantization. Table 2.2 lists the effective coherence numbers of different spin operators under different gradient pulses.

Table 2.2 Effective Coherence Numbers

	gradient x	gradient y	gradient z
Ix	0	+/- 1	+/- 1
Iy	+/- 1	0	+/- 1
Iz	+/- 1	+/- 1	0
IxIx	0	0, +/- 2	0, +/- 2
IxIy	+/- 1	+/- 1	0, +/- 2
IxIz	+/- 1	0, +/- 2	+/- 1
IyIx	+/- 1	+/- 1	0, +/- 2
IyIy	0, +/- 2	0	0, +/- 2
IyIz	0, +/- 2	+/- 1	+/- 1
IzIx	+/- 1	0, +/- 2	+/- 1
IzIy	0, +/- 2	+/- 1	+/- 1
IzIz	0, +/- 2	0, +/- 2	0

Notice that the effective coherence number is indeed a function of the axis of quantization and that any two spin state will be a combination of zero and double quantum states for at least one quantization direction.

A key feature of changing the axis of quantization is that there is a corresponding change in coherence number. We need, therefore, a manner of connecting states. For example an $I_zI'_z$ state contains only zero quantum in normal Zeeman quantization. In an x-gradient, $I_zI'_z$ contains both zero and double quantum components, if the gradient is changed to a y-gradient, there is again both zero and double quantum

terms. The complexity of these transformations (changes in direction of quantization) are revealed by expressing the various raising and lowering operators in terms of one another, as shown in table 2.3.

Table 2.3.

z-quantized	x-quantized	y-quantized
$I_x = \frac{1}{2}[I_z^+ + I_z^-]$	$I_y = \frac{1}{2}[I_x^+ + I_x^-]$	$I_x = \frac{i}{2}[I_y^- - I_y^+]$
$I_x^+ = \frac{i}{2}[I_z^- - I_z^+] + i\, I_z$	$I_y^+ = \frac{i}{2}[I_x^- - I_x^+] + i\, I_x$	$I_x^+ = I_y + \frac{i}{2}[I_y^+ + I_y^-]$
$I_x^- = \frac{i}{2}[I_z^- - I_z^+] - i\, I_z$	$I_y^- = \frac{i}{2}[I_x^- - I_x^+] - i\, I_x$	$I_x^- = I_y - \frac{i}{2}[I_y^+ + I_y^-]$
$I_y = \frac{i}{2}[I_z^- - I_z^+]$	$I_z = \frac{i}{2}[I_x^- - I_x^+]$	$I_z = \frac{1}{2}[I_y^+ + I_y^-]$
$I_y^+ = I_z + \frac{i}{2}[I_z^+ + I_z^-]$	$I_z^+ = I_x + \frac{i}{2}[I_x^+ + I_x^-]$	$I_z^+ = \frac{i}{2}[I_y^- - I_y^+] + i\, I_y$
$I_y^- = I_z - \frac{i}{2}[I_z^+ + I_z^-]$	$I_z^- = I_x - \frac{i}{2}[I_x^+ + I_x^-]$	$I_z^- = \frac{i}{2}[I_y^- - I_y^+] - i\, I_y$

Notice in particular that any raising or lowering operator when requantized along an orthogonal axis is transformed into a superposition of states with coherence numbers of zero, one and minus one.

The above tables are useful and may be employed to create tables of connectivities between product operators quantized along the various Cartesian directions, these are contained in table 2.4, 2.5, 2.6, 2.7.

Tables 2.2 and 2.3 provide all the information needed to completely explore the dynamics of any homonuclear multiple-quantum filtered experiment.

§2.5 General Multiple Quantum Filters

A general homonuclear multiple quantum filter can be constructed from two RF pulses. The first RF pulse transforms the coherence from an anti-phase state into a multiple quantum state, a portion of which is returned to an anti-phase coherence by the second RF pulse. The coherence transformations by themselves provide no selectivity, the spins must also be subjected to a coherence specific interaction in such

	I_x^+	I_x^-	I_x	$I_x^+ I_x^+$	$I_x^+ I_x^-$	$I_x^+ I_x$	$I_x^- I_x^+$	$I_x^- I_x^-$	$I_x^- I_x$	$I_x I_x^+$	$I_x I_x^-$	$I_x I_x$
I_x			1									
I_y	1/2	1/2										
I_z	-i/2	i/2										
I_xI_x												1
I_yI_y				1/4	1/4		1/4	1/4				
I_zI_z				-1/4	1/4		1/4	-1/4				
I_xI_y										1/2	1/2	
I_yI_x						1/2			1/2			
I_xI_z										-i/2	i/2	
I_yI_z				-i/4	i/4		-i/4	i/4				
I_zI_x						-i/2			i/2			
I_zI_y				-i/4	-i/4		i/4	i/4				

Table 2.4 Basis product operator transformation: Cartesian to x-quantized

a way that only a certain pathway is selected.

In phase cycling methods, this interaction is a phase shift of the RF pulses. The response of a coherence to a phase shift of the RF is proportional to its coherence number. This is easily seen by rewriting an RF pulse with arbitrary phase ϕ and rotation angle α as a combination of z-rotations and an x-pulse[24],

$$R_{\Phi,\alpha}=R_{Z,-\Delta\Phi}R_{x,\alpha}R_{Z,\Delta\Phi}$$

where $\Delta\Phi$ is the shift of the RF phase with respect to an x-pulse. A phase shift $\Delta\Phi$ of the RF pulse results in a phase shift $k\Delta\Phi$ of the spin coherence of order k. The addition of a number of experiments with a suitable combination of phase shifts leads to the desired selectivity.

The use of B_0 gradients in coherence pathway selection mimics the phase cycling methods in that the discreet z-rotations in the phase cycling case are replaced by continuous z-rotations due to the B_0 gradients. The coherence number now describes the relative rate of dephasing of a spin coherence, which becomes clear when ω is replaced

	I_y^+	I_y^-	I_y	$I_y^+I_y^+$	$I_y^+I_y^-$	$I_y^+I_y$	$I_y^-I_y^+$	$I_y^-I_y^-$	$I_y^-I_y$	$I_yI_y^+$	$I_yI_y^-$	I_yI_y
I_x	-i/2	i/2										
I_y			1									
I_z	1/2	1/2										
I_xI_x				-1/4	1/4		1/4	-1/4				
I_yI_y												1
I_zI_z				1/4	1/4		1/4	1/4				
I_xI_y						-i/2			i/2			
I_yI_x										-i/2	i/2	
I_xI_z				-i/4	-i/4		i/4	i/4				
I_yI_z										1/2	1/2	
I_zI_x				-i/4	i/4		-i/4	i/4				
I_zI_y						1/2			1/2			

Table 2.5 Basis product operator transformation: Cartesian to y-quantized

	I_z^+	I_z^-	I_z	$I_z^+I_z^+$	$I_z^+I_z^-$	$I_z^+I_z$	$I_z^-I_z^+$	$I_z^-I_z^-$	$I_z^-I_z$	$I_zI_z^+$	$I_zI_z^-$	I_zI_z
I_x	1/2	1/2										
I_y	-i/2	i/2										
I_z			1									
I_xI_x				1/4	1/4		1/4	1/4				
I_yI_y				-1/4	1/4		1/4	-1/4				
I_zI_z												1
I_xI_y				-i/4	i/4		-i/4	i/4				
I_yI_x				-i/4	-i/4		i/4	i/4				
I_xI_z						1/2			1/2			
I_yI_z						-i/2			i/2			
I_zI_x										1/2	1/2	
I_zI_y									-i/2		i/2	

Table 2.6 Basis product operator transformation: Cartesian to z-quantized

by a spatially modulated term:

$$\omega(r) = \gamma \frac{\partial B_z}{\partial r} r \quad .$$

	I_y^+	I_y^-	I_y	$I_y^+I_y^+$	$I_y^+I_y^-$	$I_y^+I_y$	$I_y^-I_y^+$	$I_y^-I_y^-$	$I_y^-I_y$	$I_yI_y^+$	$I_yI_y^-$	I_yI_y
I_x^+	i/2	i/2	1									
I_x^-	-i/2	-i/2	1									
I_x	-i/2	i/2										
$I_x^+ I_x^+$				-1/4	-1/4	i/2	-1/4	-1/4	i/2	i/2	i/2	1
$I_x^+ I_x^-$				1/4	1/4	i/2	1/4	1/4	i/2	-i/2	-i/2	1
$I_x^+ I_x$				1/4	-1/4		1/4	-1/4		-i/2	i/2	
$I_x^-I_x^+$				1/4	1/4	-i/2	1/4	1/4	-i/2	i/2	i/2	1
$I_x^-I_x^-$				-1/4	-1/4	-i/2	-1/4	-1/4	-i/2	-i/2	-i/2	1
$I_x^-I_x$				-1/4	1/4		-1/4	1/4		-i/2	i/2	
$I_xI_x^+$				1/4	1/4	-i/2	-1/4	-1/4	i/2			
$I_xI_x^-$				-1/4	-1/4	-i/2	1/4	1/4	i/2			
I_xI_x				-1/4	-i/2		-i/2	-1/4				

Table 2.7 Basis product operator transformation: x-quantized to y-quantized

The desired selectivity is achieved by dephasing a spin in one state and re-phasing the magnetization as a gradient echo after a coherence transformation which alters the coherence number of the state of interest.

In RF gradient spectroscopy, the gradient pulse is responsible for both the dephasing / re-phasing and for introducing coherence transformations. This leads to a complex mixture of spin states due to simultaneous gradient evolution and coherence transformations, but to have a convenient picture of the dynamics, it is useful to separate the two operations. Our approach to this separation is to quantize the states along the axis of the gradient field in the rotating frame, so that there are no coherence transformations during the gradient pulse. The re-quantization involves an expansion of the Cartesian single spin operators into raising and lowering operators that are quantized along I_x and I_y . When a given RF gradient field is applied:

(1) The spin system interacts as though it is quantized along the gradient field.

(2) The gradient interaction is sufficient to remove through second averaging all internal interactions.

Notice that this second point is not immediately true for RF gradient experiments employing a quadrupolar geometry gradient coil, for the field passes through zero at the center of the sample. But such fields are normally employed with coherent averaging to directly remove the internal interactions.

The requantization methodology is now clear. The essence of requantization is to separate the coherence transformation and gradient evolution(dephasing/re-phasing) process that are simultaneous happened during RF gradient period. The change of basis function allows the requantization to take the place of the coherence transformation so that after the requantization, there is no coherence transformation during the RF gradient period. Since the spin system has been requantized along the dominant RF gradient direction, the internal Hamiltonian is averaged to zero and the spin is locked along the RF gradient direction and the coherence number is preserved. Only gradient evolution effects, i.e. dephasing/ re-phasing, need to be considered, and the coherence pathway is easily followed. The reason is that, after the coherence number jumps during the requantization, the coherence numbers are preserved during the RF gradient evolution. Now, to illustrate the coherence pathway that the spin system go through, three separate pictures of the coherence numbers are required to understand both the coherence number jumps and coherence pathway selection process. These three pictures traces the coherence number along the three orthogonal axes, in the rotating plane, i.e. I_x, I_y and I_z.

2.6 Requantization Methodology and RF Gradient Multiple Quantum Filter Design

RF gradient multiple quantum filters (like B_0 gradient MQF) generally employ two gradient pulses that are of unequal length to introduce selectivity. For optimal selectivity and sensitivity, the phase

difference between the two gradient pulses must be 90° so that all spins are requantized. The implication is that all coherences experience a coherence transformation during the requantization step. A change in coherence number is a requirement for selectivity. For other phase angles, a subset of the spins will be at best simply dephased(reducing the overall sensitivity), or experience a gradient echo(reducing the selectivity).

We will arbitrarily take the first gradient to be along Ix, which will have no influence on the generality of the conclusions. In discussing MQF we are interested in variations that introduce changes in the coherence pathways. Changes in phase of the detected signal are not of particular interest.

If we restrict the discussion to RF pulses along the Cartesian axes, there is no reason to place a pulse in between the gradients since the pulse will commute with one of the two gradients and so it may be moved either before or after the gradient pulse pair, without changing the overall spin dynamics.

Just prior to the start of a multiple quantum filter, the spin magnetization is in an anti-phase state since no mixing has occurred, and under the influence of internal Hamiltonians this state would evolve into an observable in-phase coherence. The anti-phase states are either $I_xI_zI_z$.. or $I_yI_zI_z$... These are requantized along the I_x axis and hence cover a manifold of states.

An RF pulse prior to the planar RF gradient is of no interest since it does not introduce any new branching and indeed has no influence on the branching ratios.

Now, we define the branching ratio as the fraction of magnetization that flows into a particular level of coherence state during a requantization.

As seen in the figure 2.1, following the second RF gradient pulse, all states are connected to the -1 I_z state which is the only observable state. So the experiment can always be arranged to give an echo for a specific MQF in a -1 I_z state. However, not all -1 states (-1 I_x, -1 I_y) are observable since not all -1 states evolve into in-phase single spin states which are the only states that are observable in the standard dipole detection arrangement of an NMR spectrometer. RF pulses after the gradient pulse pair are occasionally useful, therefore, to create anti-phase magnetization which will evolve into observable magnetization.

The core concept of the analysis of an RF gradient experiment is the requantization of the spin system when the dominant Hamiltonian shift axes. When the spin system freely evolves, the normal Zeeman quantization is applied, and the spin system is quantized along z. However, during the RF gradient evolution, the spin system is quantized along I_x or I_y. Each requantization will introduce a multiplication function $f_{i,j}(k,l)$, where i denotes the pathway, j denotes the serial number of the requantization process, k is the old coherence number and l is the new coherence number. The multiplication function represents the redistribution of the population of each coherence order of the original quantization, and can also be called branching weight. Each time the spin system is requantized, the selected population will decrease by a multiplication factor. After the population go through a complete pathway, the contribution to the detected signal intensity from this pathway is the product of the requantization factors or branching weights, and the total signal intensity is the sum of the signal intensities generated through each pathway, i.e.

$$\text{S.I.} = \sum_{\text{pathways, i}} \prod_{\text{requantization, j}} f_{i,j}(k,l) \quad .$$

Requantization requires a change of basis operator set. For any spin system, there are four pertinent spin operator sets, the Cartesian basis (I_x, I_y, I_z), the x basis(I_x^+, I_x^-, I_x), the y basis(I_y^+, I_y^-, I_y), and the z basis (I_z^+, I_z^-, I_z).

An arbitrary spin operator can be thought of a linear superposition of the basis operators in any set. The basic problem of requantization is to change from one basis set into another basis set. Any basis operator in basis set A can be expressed in the linear superposition form of basis operators from the basis set B. Now, define the mapping factor as the coefficient of each basis operator in basis set B in the expression of a particular basis operator from basis set A. For an N-spin system, once all the mapping factors are calculated (see the table 2.4 through 2.7), the problem of requantization is solved. No matter how complicated the RF gradient experiment is, the final signal intensity can be calculated through tracing all possible pathways. Each requantization along the pathway will contribute one multiplication factor and the final signal intensity will be the sum of the products of the multiplication factors along each pathway.

2.7 RF Gradient Multiple Quantum Filter Pulse Sequence Analysis

The proposed pulse sequence(figure 2.2) for the N-quantum filter consists of two back to back gradient pulses.

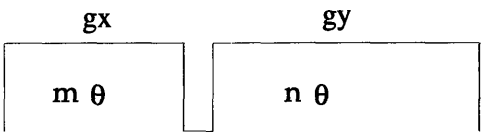

Figure 2.2 RF gradient multiple quantum filter pulse sequence.

Assume the strengths of the two RF gradients are of the same, then the duration of the two gradient pulses is in the ratio of m:n. The anti-phased term, $I_{1y}I_{2z}...I_{Nz}$, from N or more than N coupled spin system is of interest in our discussion. It passes through the two RF gradients, gx, gy. In the first RF gradient, gx, the spin system will be requantized from z to x to be along the RF gradient direction. The requantization will cause the coherence number to jump. After requantization, the coherence order will remain unchanged. There will be a phase shift at the end of the x gradient. This phase shift is proportional to the coherence number and the gradient duration. From gradient gx to

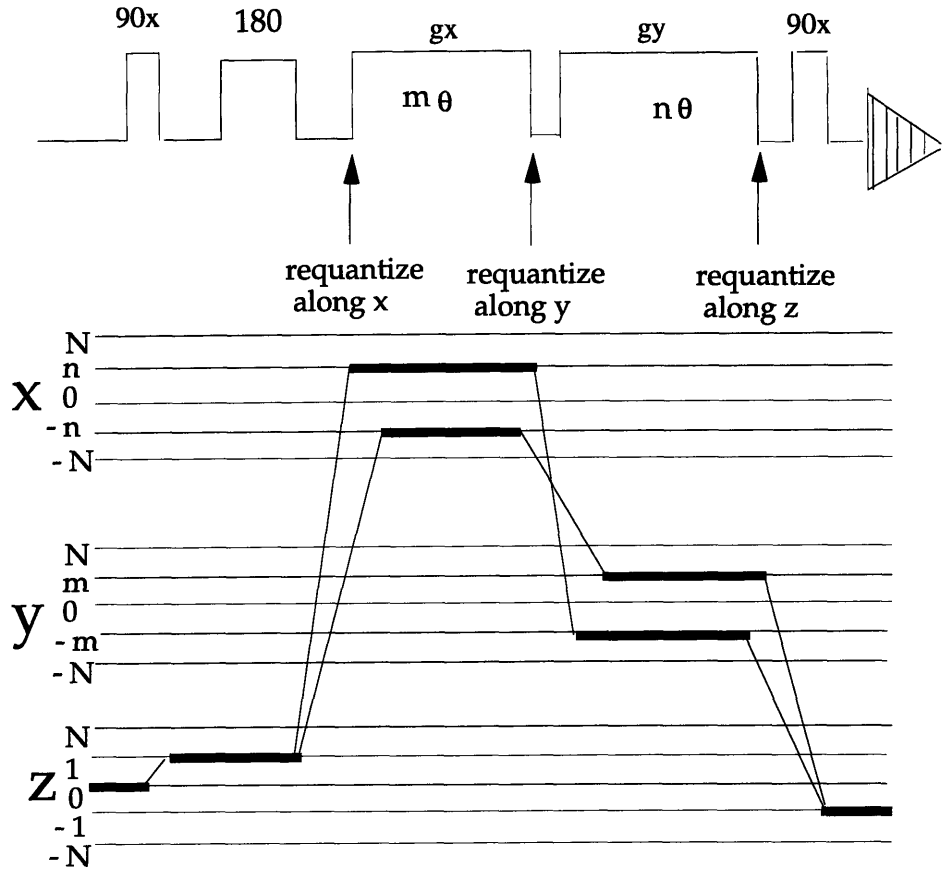

Figure 2.3 Pulse sequence and coherence diagram of a general 1-D RF multiple quantum filter Experiment.

gradient gy, there is a second requantization from I_x to I_y, since the gradient direction has changed from I_x to I_y. There is another coherence order jump accompanying the requantization. During the gx gradient, the desired coherence order is n (-n), and during the gy gradient, the desired coherence order is -m (m), and if the phase evolution during the two gradient pulse periods are equal in amplitude and opposite in sign, the total phase accumulation will be zero, or the phase is completely refocussed, and an echo may be observed.

accumulated phase = (gradient length) times (coherence number)

Figure 2.3 is the pulse sequence and coherence diagram of 1-D (or 2-D COSY, if the evolution time after the first 90° pulse is incremental

during the experiment) multiple quantum filter experiment. The first 90° pulse excites the spin system into the transverse plane. Then the spin system evolves under the scalar coupling Hamiltonian and develop into anti-phased single quantum coherence. The two RF gradient pulses act as a multiple quantum filter to select certain spin systems and block others.

An analysis of the above pulse sequence and the related coherence diagrams demonstrate general properties of a Multiple Quantum Filter. First, the coherence number must be N during one gradient duration, in order to achieve the desired selectivity.

Second, the coherence pathway selection depends on the ratio of the product of the gradient strength and the gradient duration of the two RF gradients. Their absolute strength or duration is not important as long as the gradient strengths are strong enough so that the RF gradient Hamiltonian dominates all the internal Hamiltonians.

In a phase sensitive experiment, TPPI(Time-Proportional-Phase-Incrementation)[2.1] is usually used to allow phase sensitive in the ω1 direction. This is convenient achieved through 90° phase increment of the first 90° pulse throughout the experiment. With TPPI, only one of the spin state, $I_{1z}{}^{+}I_{2z}...I_{Nz}$, or $I_{1z}{}^{-}I_{2z}...I_{Nz}$ is selected during t_1 evolution. A high resolution lineshape is observed if the +1 coherence is selected during t1. Then there are only two coherence pathways possible, in one, the spin state will go through a state of coherence number n during gx gradient period, and then a state of coherence number (- m) during gy gradient period, and in the other, the spin state will go through a state of coherence number (-n) during gx gradient period, and then a state of coherence number m during gy gradient period.

Third, for an RF gradient N-quantum filter, one of the gradient duration (m, or n) has to be N, and the other may be any integer, which has no common multiplication factors with N. Such N-quantum filter will only select spin systems with N or more coupled spins.

Fourth, for an RF gradient N-quantum filter, if N is a primary number, the other gradient duration can be any integer, since a primary number has no common multiplication factor with other integers.

Fifth, the signal efficiency depends on the population of spins that goes through the coherence pathways. It can be shown that the lower the absolute value of the coherence number of the spin, the larger the population, and the higher the efficiency of the multiple quantum filter.

Based on the above discussion, there are always four gradient combinations that will achieve an N-filters,

(1). m = 1, n = N
(2). m = N, n = 1
(3). m = N-1, n = N
(4). m = N, n = N-1

The (1,N) combination will have the highest efficiency, the ((N-1),N) case will require the least pulses, i.e. only the gradient pulse, and the (1,N) case will need additional 90° pulses. These 90° pulses not only make the necessary coherence order jumps possible, but also make the requantization process the more efficient.

N-quantum filters and their efficiencies.

m	n	Initial state	final state	pulse sequence	efficiency
N-1	N	$I_{1z}{}^{+}I_{2z}...I_{Nz}$	$\Sigma_{\kappa}I_{1z}..I_{kz}{}^{-}..I_{Nz}$	seq. #1	$(1/2)^{2N-1}$
1	N	$I_{1z}{}^{+}I_{2z}...I_{Nz}$	$\Sigma_{\kappa}I_{1z}..I_{kz}{}^{-}..I_{Nz}$	seq. #2	$(1/2)^{N+1}$

Discussions on two N-quantum filters.

Case 1. m = N-1, n=N.

Figure 2.4 is the pulse sequence (seq. #1) and the coherence pathway.

As mentioned earlier, the signal intensity is the product of the branching weights(f11, f21, etc.) along each coherence pathway and finally summed over all coherence pathways.

Signal intensity = | f11 f21 f31 + f12 f22 f32 |

$$=((i/2)^{N}(-1)^{N-1}(i/2)^{N-1}(i/2) + (i/2)^{N}(i/2)^{N-1}(-1)^{N-1}(i/2))$$

$$=(1/2)^{2N-1}$$

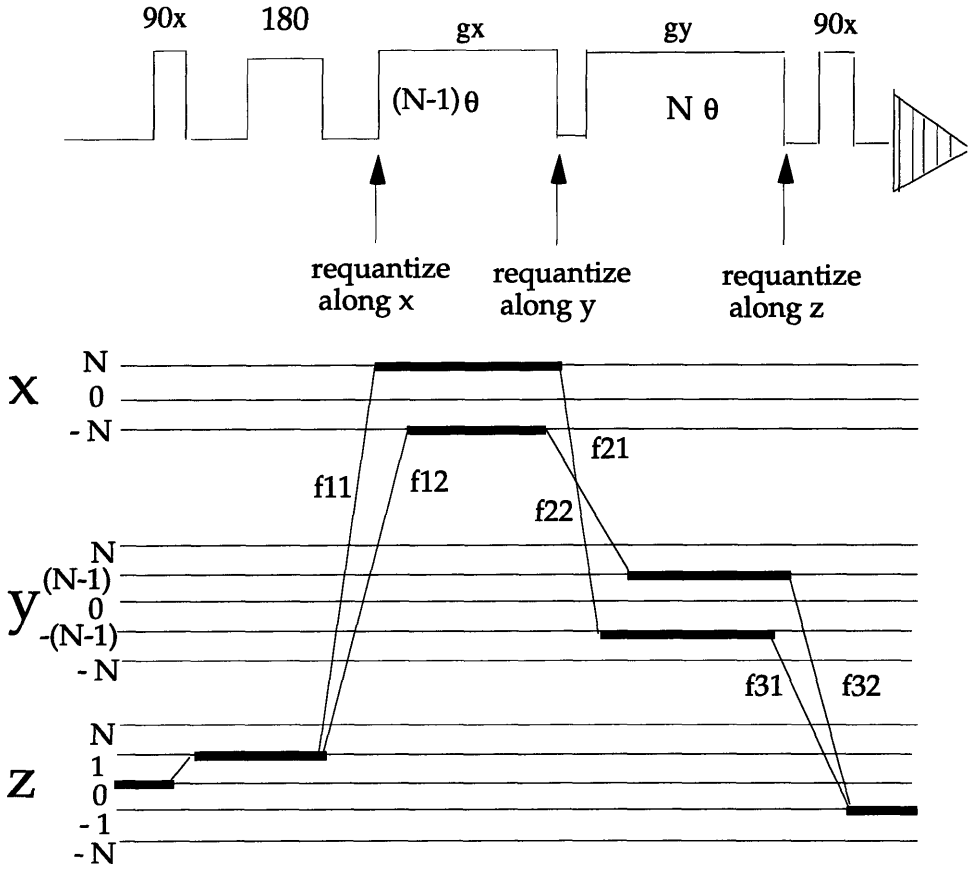

Figure 2.4 1-D RF gradient multiple quantum filter Experiment: (N-1, N) case.

Case 2. m = 1, n=N.

Figure 2.5 is the pulse sequence (seq. #2) and the coherence pathway.
Signal intensity = | f11 f21 f31 + f21 f22 f32 | = $(1/2)^{N+1}$

The last $90°_x$ pulse makes the following coherence transfer pathway possible:

$$I_{1y}{}^{-}I_{2y}...I_{Ny} \quad \text{---------- } 90°x \text{ ---------> } (-i)\, I_{1z}{}^{-}I_{2z}...I_{Nz}$$

The $90°_x$ is a rotation of the coordinate system which rotates y spin operators into single quantum z spin operators, and facilitates the detection.

$$I_{1y}{}^{-}I_{2y}...I_{Ny}=(I_{1z}-iI_{1x})I_{2y}...I_{Ny}\text{-------}90°x\text{------>}-(I_{1y}+iI_{1x})I_{2z}...I_{Nz}=(-i)I_{1z}{}^{-}I_{2z}...I_{Nz}$$

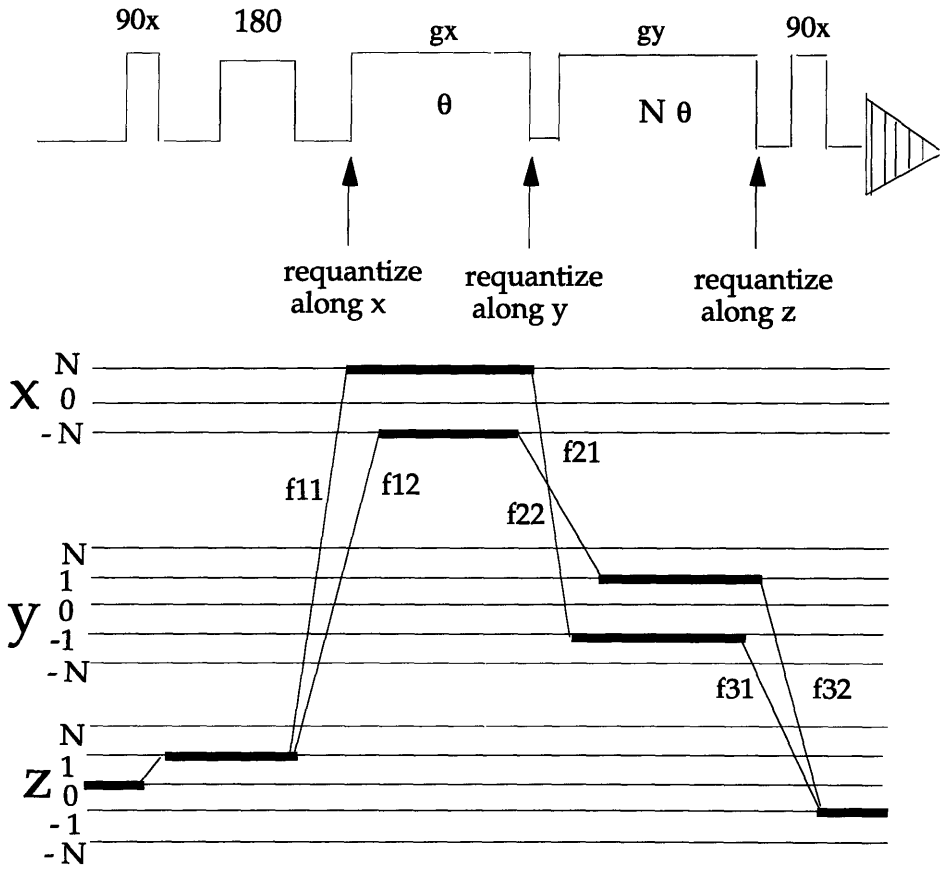

Figure 2.5 1-D RF gradient multiple quantum filter Experiment: (1, N) case.

Chapter Three

RF gradient Multiple Quantum Filters and Multiple Quantum Filtered Spectra

§3.1 RF Gradient Multiple Quantum Filters

In last chapter, RF gradient multiple quantum filters were used to illustrate the effectiveness of requantization methodology. A generalized RF gradient multiple quantum filter is designed with the help of such methodology. In this chapter, four special cases of the RF gradient multiple quantum filters are analyzed in detail and the result is compared with spectra acquired on an AMX 400 spectrometer. The experiments confirmed the theoretical result.

§3.2 RF Gradient Triple Quantum Filters

A triple quantum filter selects spins systems with three or more scalar coupled spins. Such filters can be inserted into any pulse sequence to achieve selectivity. From the generalized RF gradient multiple quantum filters, such a filter contain two back to back RF gradient pulses with 90° phase shift. The effective gradient duration of the two gradient pulses are in the ratio of 1:3. A 90°x pulse is applied at the end to convert the single quantum y-quantized coherence into single quantum z-quantized without loss of sensitivity. The pulse sequence is,

As usual, the first 90° pulse excites the spin system into transverse plane. A single quantum term I_{1y} is created by the first 90°x pulse. The

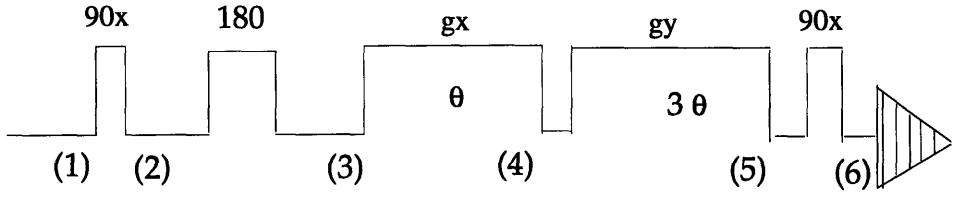

Figure 3.1 The pulse sequence of RF gradient triple quantum filter (Version 1).

spin system will evolve for a time t_1 under the scalar coupling Hamiltonian and the chemical shift Hamiltonian. For a two dimensional COSY experiment, the chemical shift labeling during t_1 is important to differentiate the different resonance peaks. In one dimensional case, a 180° pulse is inserted equal distance between the first 90° pulse and the first gradient pulse to refocus the phase distortion caused by the chemical shift and static magnetic field inhomogeneity. During t_1 evolution, the spin system is naturally quantized along z. During the first gradient pulse, the spin system is requantized along I_x, the direction of the RF gradient pulse. The spin system reaches coherence number 3. During the gradient, the triple quantum coherence evolves three times as fast as a single quantum coherence. We will see that the phase distortion accumulated during the first RF gradient pulse will be refocused by the second RF gradient pulse. The second RF gradient pulse is applied immediately after the first one. The purpose of the second pulse is to selectively re-phase the triple quantum coherence and leave single quantum coherence and double quantum coherence dephased. A requantization is necessary to transform the triple quantum coherence into a single quantum coherence for phase correction. During the second RF gradient period, the single quantum coherence is not necessary for phase correction. As we will see, a double quantum coherence with adequate effective evolution time is also possible. In general, any coherence number which is smaller that the first coherence number and is prime to the first one is a good choice. Since the coherence number of the selected spin system during the second RF gradient period is only 1/3 of the coherence number of the same spin system during the first RF gradient period, the effective gradient duration of the second period needs to be three times as long as the first gradient period to completely refocus the phase distortion caused by the evolution during the first RF gradient period. The last 90° pulse is used to convert the I_y quantized single quantum into z quantized single quantum, without sensitivity loss, to be detected in the dipole magnetic RF coil.

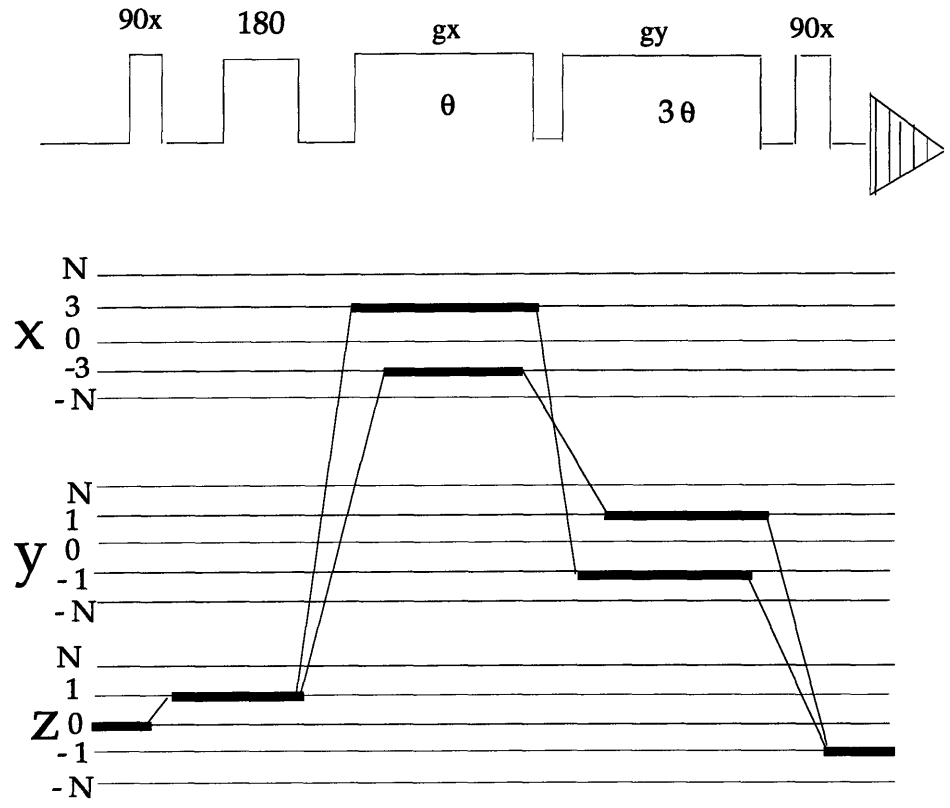

Figure 3.3 The pulse sequence and coherence diagram of RF gradient triple quantum filter (Version 1). Gradient ratio is 1:3.

The coherence diagram of the RF gradient triple quantum filter consists of three quantization axis. Each time the requantization occurs, the coherence is represented in the new quantization axis. During the RF gradient period, the coherence number is three and jumps back to one during the second RF gradient duration for phase correction. Figure 3.3 is the pulse sequence and the coherence diagram.

From the sensitivity analysis of a general RF gradient multiple quantum filter, the sensitivity of this RF gradient triple quantum filter is calculated,

Detected magnetization = $(1/2)^{3+1}$ = 1/16 of initial magnetization

The triple quantum filter (RF gradient version 1) is tested on Bruker AMX400 spectrometer, operating at a proton frequency of 400 MHz, and with a planar RF gradient field with a strength of $10Gcm^{-1}$. Proton anti-phase coherences are generated by a $\pi/2$-τ-π-τ sequence, in which τ is set to 1/(4J) (30ms). The sample is ethyl acetate(figure 3.4) in deuterated acetone.

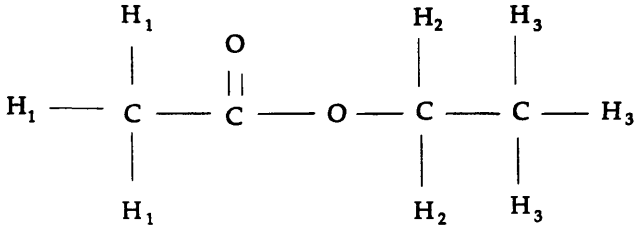

Figure 3.4 Ethyl acetate

The three methyl protons bonded to the carboyl are magnetic equivalent and they coupled to no other H spins. So they can only create single quantum coherence and give rise to single peak in the proton NMR 1-D spectrum. The methylene of the ethyl group is coupled to the three methyl protons and can create up to four quantum coherence and give rise to four peaks (intensity distribution of 1:3:3:1) in the proton NMR spectrum. The CH_3 of the ethyl group is coupled to the methyl protons and can create up to triple quantum coherence and gives rise to three peaks (intensity distribution of 1:2:1) in the proton NMR spectrum. Figure 3.5 is the 1D hydrogen NMR spectrum of ethyl acetates.

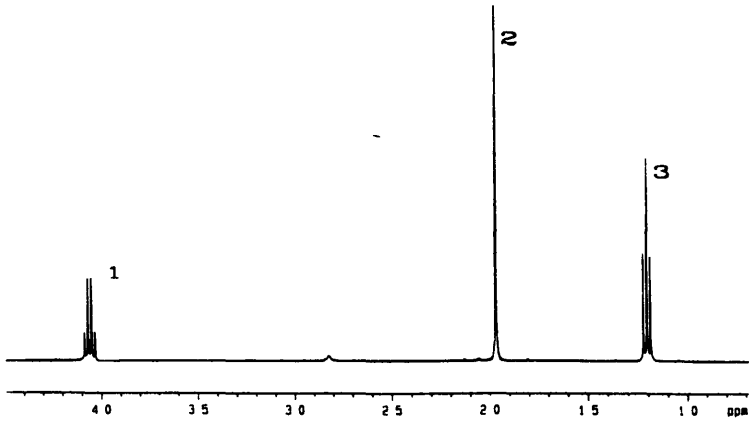

Figure 3.5 400MHz proton NMR spectrum of ethyl acetate. The resonance marked 1,2, and 3 are from the methylene, methoxy, and methyl protons, respectively.

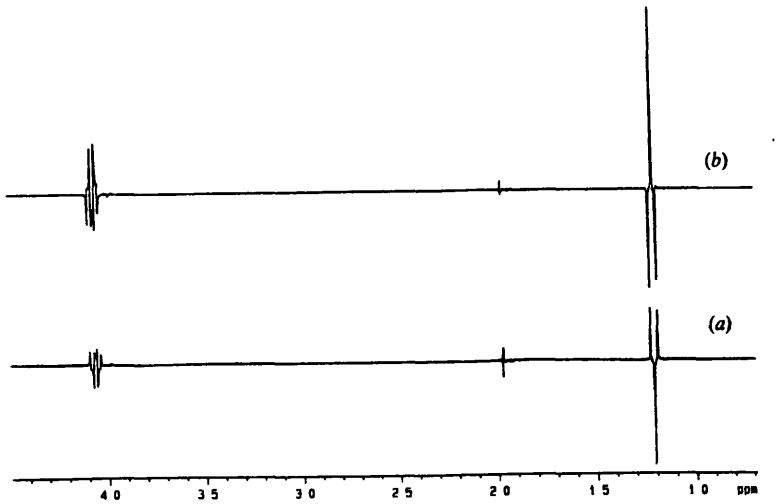

Figure 3.6 Triple quantum filtered spectra of ethyl acetate, obtained with an RF gradient combination m=2, n=3 (a) and m=1, n=3 followed by a $\pi/2$ pulse (b). A single experiment is acquired with an RF gradient with a strength 10G/cm and a unit duration of 600 μs (total gradient time 3.0 ms for (a) and 2.5 ms for (b)).

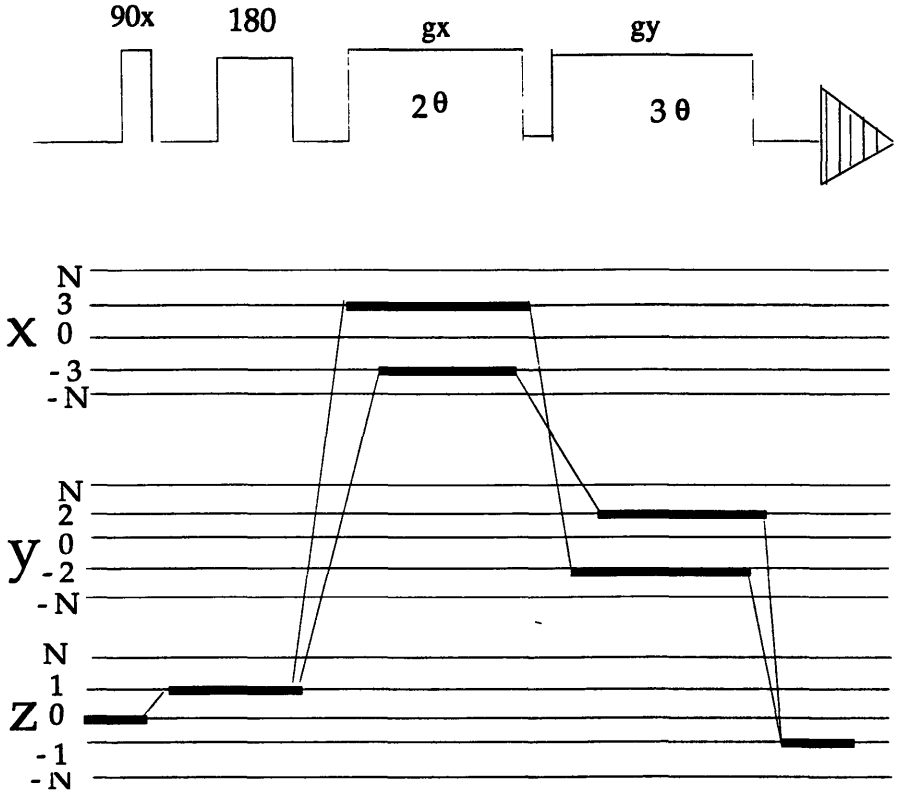

Figure 3.7 The pulse sequence and coherence diagram of RF gradient triple quantum filter (Version 2). Gradient ratio is 2:3.

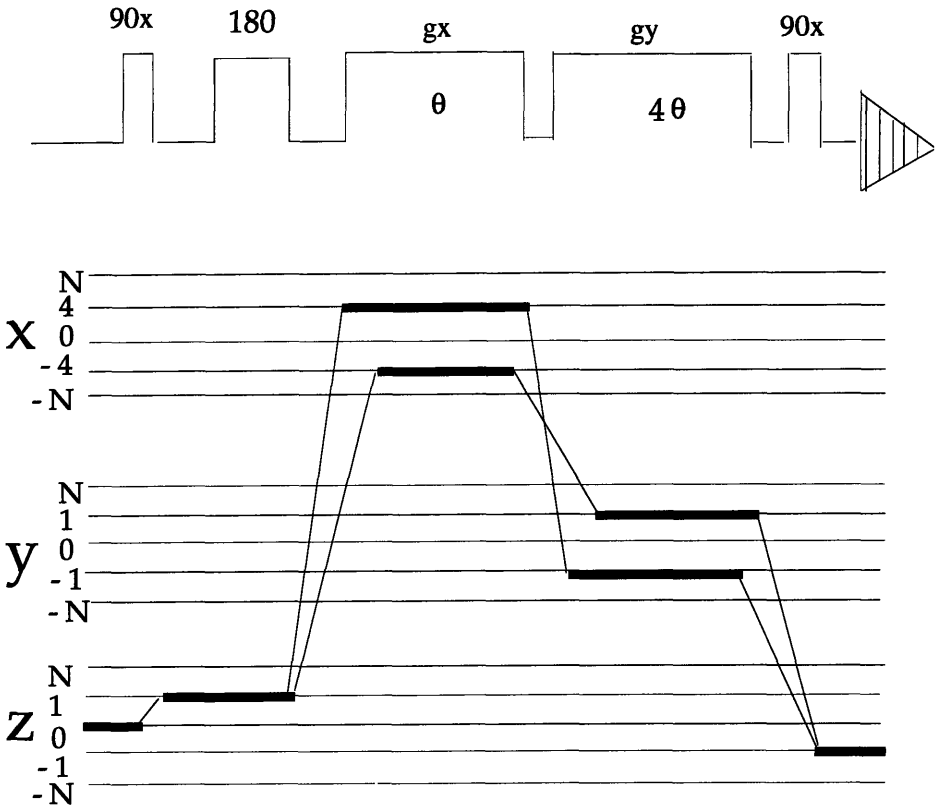

Figure 3.8 The pulse sequence and coherence diagram of RF gradient four quantum filter (Version 1). Gradient ratio is 1:4.

Figure 3.6(b) is the one dimensional RF gradient triple quantum filter spectrum of ethyl acetate.

As indicated earlier, the coherence number during the second RF gradient period can be 2 instead of 1. This minor change gives rise to anther triple quantum filter, where the effective duration of the two back to back RF gradient is 2:3. Figure 3.7 is the pulse sequence and the coherence diagram.

The sensitivity can be calculated through the formula that we got in Chapter two.

Detected magnetization = $(1/2)^{2*3-1}$ = 1/32 of initial magnetization

The triple quantum filter (RF gradient version 2) are tested on AMX400 spectrometer. A spectrum with sample ethyl acetate in deuterated acetone is shown in Figure 3.6(a).

§3.3 RF Gradient Four Quantum Filters

Figure 3.8 is the pulse sequence of the RF gradient four quantum filter(RF gradient version 1) with the corresponding coherence order diagram.

As earlier, the sensitivity is calculated,

Detected Magnetization = $(1/2)^{4+1}$ = 1/32 of initial magnetization.

The four quantum filter (RF gradient version 1) was tested on AMX400 spectrometer. Figure 3.9(b) is the spectrum with sample ethyl acetate in deuterated acetone.

A second version of the four quantum filter (RF gradient version 2) is shown in figure 3.10. As earlier, the sensitivity is calculated,

$$\text{Sensitivity} = (1/2)^{2*4-1} = 1/128 .$$

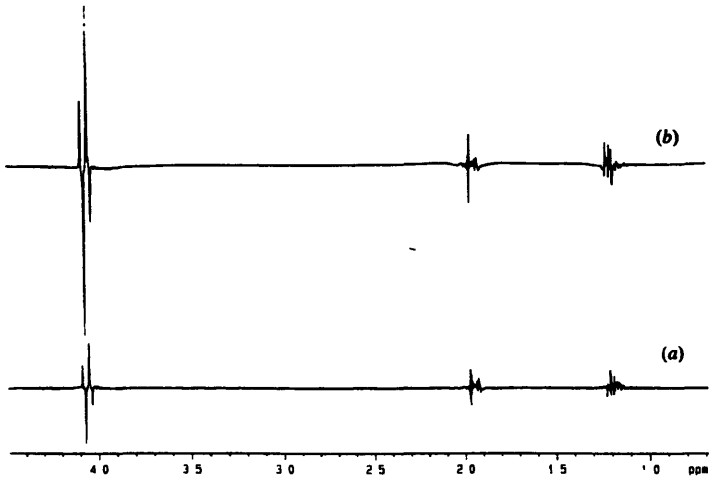

Figure 3.9 Four quantum filtered spectra of ethyl acetate, obtained with an RF gradient combination m=3, n=4 (a) and m=1, n=4 followed by a $\pi/2$ pulse (b). A single experiment is acquired with an RF gradient with a strength 10G/cm and a unit duration of 500 μs (total gradient time 3.5 ms for (a) and 2.5 ms for (b)).

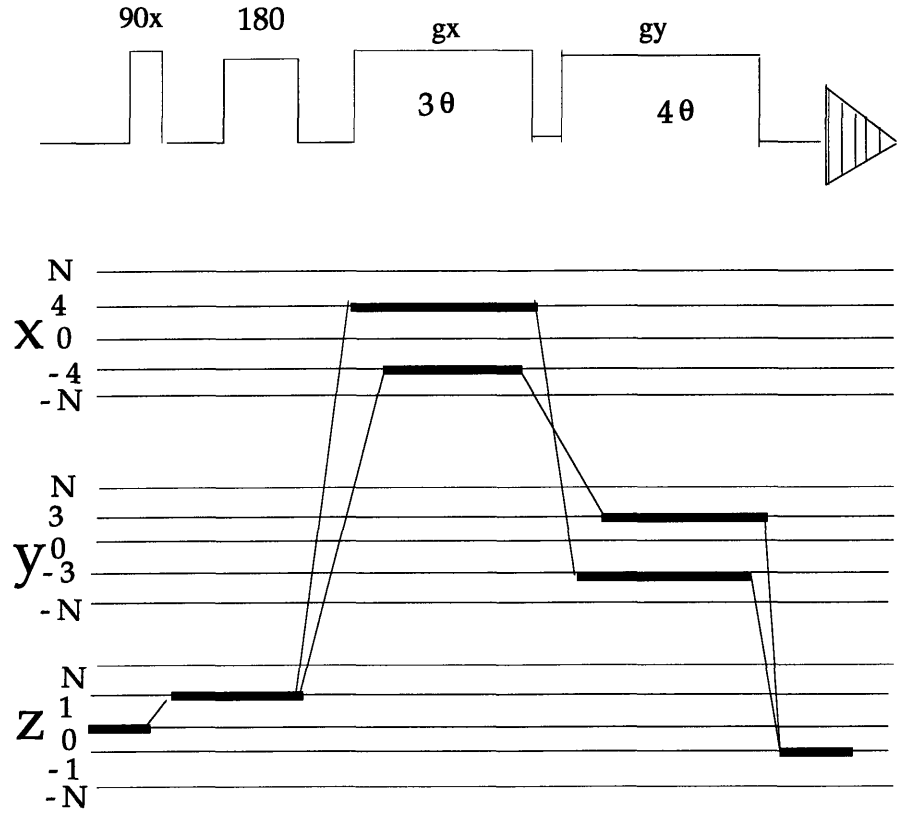

Figure 3.10 The pulse sequence and coherence diagram of RF gradient four quantum filter (Version 2). Gradient ratio is 3:4.

The four quantum filter (RF gradient version 2) has sensitivity of only 1/4 of that of the four quantum filter (RF gradient version 1). But version 2 uses less pulses.

The four quantum filter (RF gradient version 2) was tested on AMX400 spectrometer. Figure 3.9(a) is the proton spectrum with sample ethyl acetate in deuterated acetone.

Chapter Four

Multiple Quantum Filter Correlation Experiments and Other RF Gradient Experiments

§4.1 Two Dimensional RF Gradient Experiments

Multiple quantum filters are widely used to simplify complex and crowded two-dimensional spectra. A multiple quantum filter added to a COSY experiment suppress the diagonal signals, especially the solvent peak. A double quantum filter only allows the spin systems with two or more coupled spins to pass through. The uncoupled spins, especially that of the typical solvents, only create single quantum coherence state. Higher multiple quantum filters are also used to eliminate signal contributions from spin systems that consists of fewer spins. This further simplifies the spectra and makes it easier to identify the coupled spin networks.

§4.2 Advantages of RF Gradient Experiments

From the spectroscopy point of view, the main advantages of using gradients for implementing multiple quantum filters are:

1. Avoid dynamic range problems associated with the proton resonance of water since these are suppressed prior to data acquisition. This is one of the major contribution of gradient method to solvent suppression. In phase cycling experiment, the FID signal from the strong solvent resonance is not eliminated in each FID data acquisition, it is eliminated in the post processing of the different scans of the same experiment with phase shifted pulse sequence. In each scan, the ADC (Analog-to-Digital Converter) must correctly digitize the strong solvent resonance signal and the dynamic range of the signal from the resonance of molecules of interests is therefore limited. Compared to the time-averaging of phased methods, gradient spectroscopy incorporates the concept of spatial averaging, i.e. the coherence selection is done through space. In a gradient version of double

quantum filter, the desired double quantum is refocused across the space and the undesired single quantum (e.g. from water resonance) will be averaged to zero across the sample. During the data acquisition period, the total dynamic range of the ADC is occupied by the signal from the resonance of molecules of interests and the signal-to-noise ratio is also higher, since the first stage of the pre-amplifier may be set to a higher gain.

2. Solvent suppression is significantly less dependent on the line shape and therefore the shimming. Also, resonance under the solvent and resonance that exchange with the solvent can be observed. In water presaturation scheme, the maximum degree of H_2O suppression depends on the line shape and the line width of the H_2O and on the RF field strength of the soft pulse. The higher the RF power of the soft pulse, the wider the bandwidth where signals are suppressed. Poor shimming will generate poor line shape with broad line width, which may overlap with nearby signal spectrum and leads to failure of presaturation scheme.

In case of a gradient double quantum filter experiment, all of the single quantum coherences will be eliminated and the double quantum coherence will be preserved, regardless of their position in the spectrum and regardless of the width of the single quantum peak. This elegant nature of the double quantum filter makes it possible to study spin resonance that have the same resonance frequency as the water resonance.

3. Gradient methods lead to a significant reduction in t_1 noise. The introduction of t_1 noise is due to variation of the experimental conditions from acquisition to acquisition in a 2D sequence, which in turn, leads to irregular fluctuations of the signal intensity as a function of t_1. A gradient multiple quantum filter selects the relevant coherent transfer pathways in a single step and thereby eliminates t_1 noise.

4. In gradient enhanced methods, multi-dimensional experiments can be acquired in a single acquisition as compared to phase cycling

methods, where a number of FIDs generated through the similar pulse sequence with phase-shifted pulses must be added together to select the signal of interest. In gradient experiment, the desired coherence pathway is selected in a single scan. For certain experiments, gradient methods can save valuable machine times when small molecules are studied. When large molecules are studied, the typical low solubility of the molecules requires many scans to achieve an adequate signal-to-noise ratio, and gradient methods do not save time.

In addition to the advantage of gradient methods, RF gradient spectroscopy has many potential advantages over B_0 gradient methods.

(1) In heteronuclear experiments, B_0 gradient influences both the ^1H and X nucleus and so the two spin states must be brought into an I_zS_z state to be free of any evolution by the gradient. With an RF gradient there is more flexibility since the gradient will only influence the ^1H spins and the gradient can be oriented anywhere in the transverse plane (Brondeau et al. 1992).

(2) The RF field is non-secular, and therefore RF gradients can average out internal interactions and hence interrupt spin evolution save that from the gradient itself. Since every gradient requires some time, in the B_0 gradient case, phase evolution continue during the gradient pulse and extra steps must be included in the pulse sequence to refocus this evolution. With RF gradients the RF field is orthogonal to the internal Hamiltonians and if the gradient is sufficiently strong, all internal Hamiltonians are second averaged to zero, resulting in no net phase evolution during the gradient pulse. Phase sensitive RF gradient methods therefore retain the simplicity of phase cycled sequences, while their B_0 counterparts generally include extra refocusing pulses and intervals.

(3) In the presence of an RF gradient, the magnetization is not dephased by simply T_2 relaxation, since it is either spin locked during

the gradient period(decays as $T_{1\rho}$), or it decays as a combination of T_1 and T_2.

(4) Since B_0 gradients are along the axis of quantization, they can not introduce a coherence transformation themselves and must be sandwiched between RF pulses, however RF gradients are non-secular and do introduce coherence transformations. This may be accomplished in two ways, either by nutating the magnetization that is transverse to the gradient field (Canet et al. 1991), or by translating the magnetization along a swept RF field (Titman et al. 1990). The first experiment of nutating the magnetization is comparable to the dephasing/rephasing experiments of B_0 gradients except that the implementations are much more straightforward, and no phase evolution problems are encountered. The swept RF field methods are unique to RF gradient method and represent a new flexibility in designing pulse sequences. They combine the sensitivity of the spin-locking experiments (that preserve the desired magnetization along the gradient field while dephasing all transverse magnetization) with a coherence transformation step. The spins are locked along an effective gradient field, and then this is swept adiabaticly to a new location in spin space. Because there is complete flexibility in choosing both the offset and the phase of the spin locking field, the effective field can start anywhere in spin space and end up anywhere else in spin space. The phase coherence of the transverse signals depends on the path taken.

(5) Unlike the B_0 gradient, the RF gradient pulse does not disturb the spectrometer's lock channel.

(6) RF gradient's rise and fall time are very short since there are no eddy currents and the gradient coils have low inductance.

§4.3 Implementations: Planar Gradient Field vs. Quadrupolar Gradient Field

Two implementations of an RF gradient field have been explored, a planar field and a quadrupolar field. The field distribution of a planar field is shown in figure 4.1.

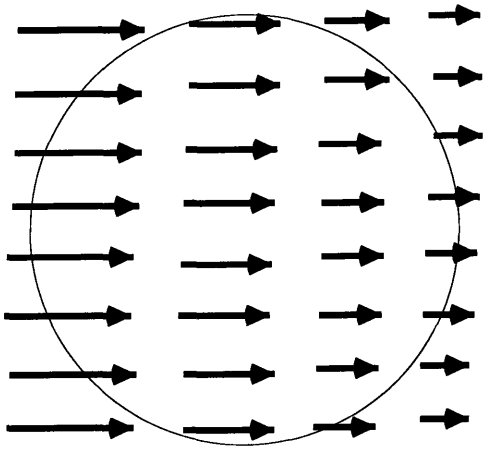

Figure 4.1 Planar RF gradient field profile.

The gradient strength changes along one selected direction, and the phase of the RF gradient is uniform through out the sample. The result is that the nutation axis of the spin doesn't change, while the nutation angle increases linearly across the sample.

A quadrupolar RF gradient field can be achieved through the configuration shown in figure 4.2.

The RF gradient field within the concentric annular rings of the sample has a constant magnitude, but the phase of the field varies over 360°. Therefore, the nutation angle is the same for every spin in the annular ring, and the nutation axis varies over 360°.

The gradient strength in different concentric annular rings varies linearly within the radius. In the center, the intensity is zero.

Since the spins at different location of the sample experience different gradient intensities and phases, the dynamics are rather complex and after coherence averaging methods are employed to

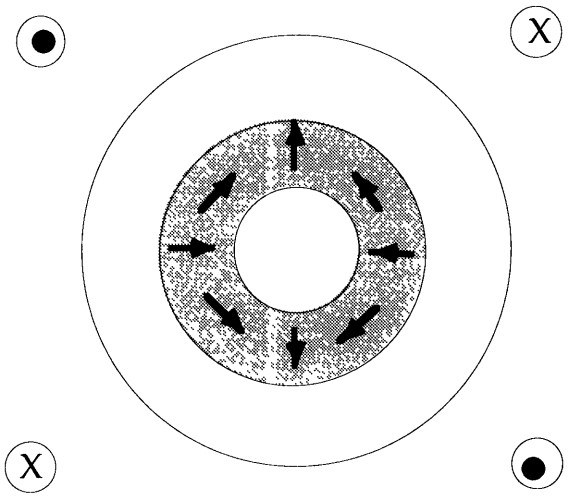

Figure 4.2 Quadrupolar RF gradient field coil configuration and field profile.

convert a quadrupolar field to a planar field.

To generate a strong RF gradient requires an additional RF gradient coil, and the alignment of the two coils creates technical problems. Another approach to generate an RF gradient field is to use the residual RF field inhomogeneity in any RF coil. The actual field that a real RF coil generates may be thought of as a superposition of a homogeneous RF field, and a residual inhomogeneous RF field. This residual RF field is convenient to use as long as the gradient time is sufficiently long so that the small inhomogeneity will completely dephase the undesired signal.

Chapter Five

RF Gradient Multiple Quantum Spectra

5.1 Introduction to the Multiple Quantum Spectrum

In Fourier NMR spectroscopy, only single quantum coherence can be observed directly. Multiple quantum coherence, however, can be observed indirectly, by using two-dimensional methods to phase encode the multiple quantum evolution and then detect single quantum coherences along the frequency encoded axis. Two of the important applications of multiple quantum coherences are briefly discussed below.

1 Characterization of coupled spin networks. Multiple quantum coherences evolve as a collected motion of a set of coupled spins, where one is interested in the chemistry and dynamics of a specific group of spins, it is possible to design a pulse sequence to excite and detect the specific spin network[5.1].

2 Zero quantum coherences evolve independent of any magnetic field inhomogeneities, since the difference frequency of two spins removes the field offset term which is common to both. This feature permits the acquisition of high-resolution spectra in even inhomogenous magnetic fields.

Multiple quantum coherences in weakly coupled spin systems can be represented through a product of raising and lowering operators (I^+, I^-). The coherence $|a\rangle\langle b|$ can be represented by the following:

$$|a\rangle\langle b| = \prod_{k=1}^{q} I_k^j \quad ,$$

where j =0, +, -. In the above expression, we assume that the spin system has a total of p spins, q of them are active and (p-q) of them are passive. The coherence $|a\rangle\langle b|$ precesses with frequency ω_{ab} :

$$\omega_{ab} = \sum_{\substack{k \\ \text{active}}} \Omega_k \Delta M_k + \sum_{\substack{k \\ \text{active}}} \sum_{\substack{l \\ \text{passive}}} 2\pi J_{kl} \Delta M_k M_l$$

where $\Delta M_k = 1, -1$, and $M_l = 1/2, -1/2$.

The effective resonance offset (or effective chemical shift [5.3]) of the multiple quantum coherence is,

$$\Omega_{eff} = \sum_{\substack{k \\ \text{active}}} \Omega_k \Delta M_k \quad .$$

There is an observable coupling between the active spins and the passive spins with a coupling constant of,

$$J_{eff} = \sum_{\substack{k \\ \text{active}}} J_{km} \Delta M_k \quad .$$

Coupling between active spins or between passive spins are not observable.

Multiple quantum coherences can be represented by raising and lowering operators, or by Cartesian operators, as illustrated below for double quantum and zero quantum coherences.

$$(2QT)_x = \frac{1}{2}(I_1^+ I_2^+ + I_1^- I_2^-) = \frac{1}{2}(2I_{1x} I_{2x} - 2I_{1y} I_{2y})$$

$$(2QT)_y = \frac{1}{2i}(I_1^+ I_2^+ - I_1^- I_2^-) = \frac{1}{2}(2I_{1x} I_{2y} + 2I_{1y} I_{2x})$$

$$(ZQT)_x = \frac{1}{2}(I_1^+ I_2^- + I_1^- I_2^+) = \frac{1}{2}(2I_{1x} I_{2x} + 2I_{1y} I_{2y})$$

$$(ZQT)_y = \frac{1}{2i}(I_1^+ I_2^- - I_1^- I_2^+) = \frac{1}{2}(2I_{1y} I_{2x} - 2I_{1x} I_{2y})$$

Similarly, arbitrary p-spin-qQT coherence can be defined. The precession under the effective chemical shift Hamiltonian and effective J-coupling Hamiltonian is similar to that of single quantum coherence,

$$(\text{p-spin-qQT})_x \rightarrow (\text{p-spin-qQT})_x \cos(\Omega_{eff}t) + (\text{p-spin-qQT})_y \sin(\Omega_{eff}t)$$

$$(\text{p-spin-qQT})_x \rightarrow (\text{p-spin-qQT})_x \cos(\pi J_{eff}t) + 2I_{mz}(\text{p-spin-qQT})_y \sin(\pi J_{eff}t)$$

§5.2 Multiple Quantum Coherence Spectroscopy with Phase Cycling

The pulse sequence for an n-quantum coherence spectrum is shown in figure 5.1.

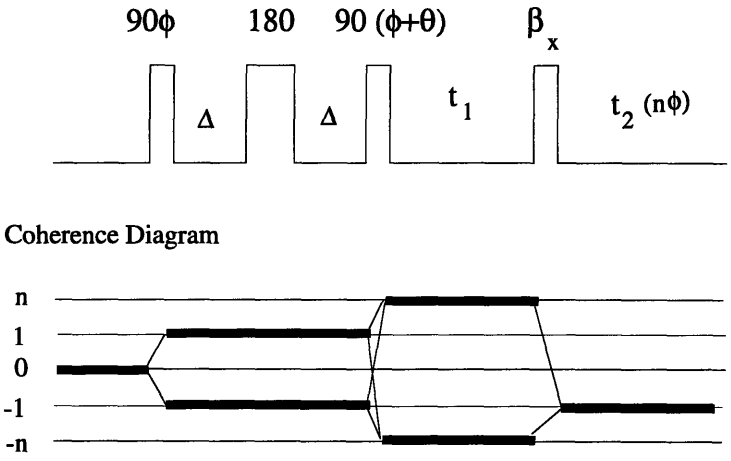

Figure 5.1 Pulse sequence and coherence diagram of the phase cycled multiple quantum coherence spectroscopy, where $\theta=(n \bmod 2)\ 90°$, and $\phi=k(\pi/n)$, with $k=0,1,\ldots,2n-1$.

The first 90° pulse excites the spin system. The following delay (2Δ) allows the in-phase single quantum coherence to evolve into anti-phase single quantum coherence. The 180° pulse in the middle is used to reverse the evolution under linear I_z Hamiltonians (chemical Shift, B_0 field inhomogeneity) so that the evolution under these linear I_z Hamiltonians are refocussed. The delay (2Δ) is selected to be $1/(4J)$ so that most of the coupled spins evolve into anti-phase single quantum coherence. The second 90° pulse is applied to convert the anti-phase

single quantum into multiple quantum coherences. The multiple quantum coherences evolve during t_1, and the last pulse converts the multiple quantum coherence back into single quantum coherence for detection. Phase cycling is used to select the n-quantum coherence.

§5.3 Static Field Gradient Zero Quantum Coherence Spectroscopy

To better understand the RF gradient zero quantum coherence spectroscopy, it is interesting to look at the static field gradient zero quantum coherence pulse sequence first. A preparation pulse train 90°-Δ-180°-Δ-90° should be applied up front to excite the spin system and prepare the z-quantized multiple quantum coherence from the coupled spins. Then, they evolve during an incremental period, t_1. If non-zero quantum coherences are suppressed during the evolution period, only pure zero quantum coherences will appear along ω_1. To suppressed the non-zero quantum coherence spectrum, a B_0 gradient may be applied during the t_1 evolution period to dephase all non-zero quantum coherences. The B_0 gradient Hamiltonian can be represented as the following (from chapter one):

$$H_{B_0} = \gamma \frac{\partial B_0}{\partial z} z I_z \quad ,$$

where $\frac{\partial B_0}{\partial z}$ is the gradient strength along the z axis. The spins at different spatial locations (x,y) will evolve with different frequency and gradually become out of phase with each other. In other words, the magnetic field inhomogeneity introduced by the B_0 gradient dephases spins at different spatial locations of the sample. No additional B_0 gradient field need be applied to refocus the phase dispersion zero quantum coherence was not dephased. The corresponding gradient zero quantum coherence spectroscopy pulse sequence and coherence diagram is shown is figure 5.2.

The $90°_x$-180°-$90°_x$ builds up the zero quantum coherences contained in $I_{1x}I_{2y}$,

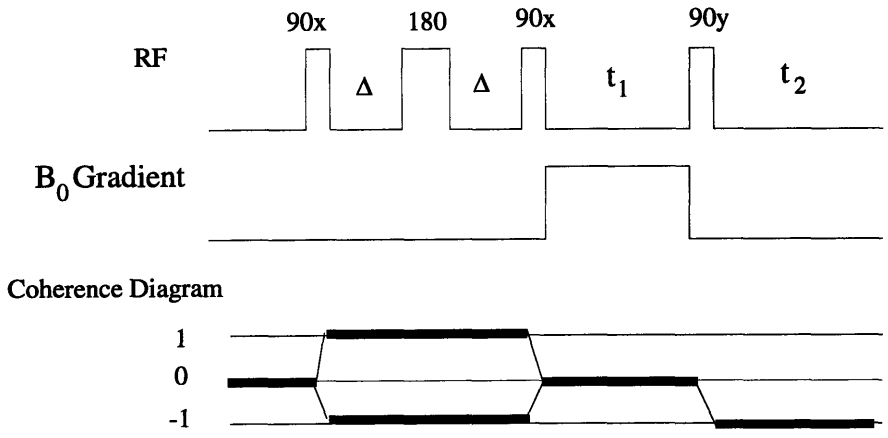

Figure 5.2 Pulse sequence and coherence diagram of the B_0 gradient zero quantum coherence spectroscopy.

$$I_{1x}I_{2y}=\left(\frac{I_1^+ + I_1^-}{2}\right)\left(\frac{I_2^+ - I_2^-}{2i}\right)=\frac{I_1^+I_2^+ - I_1^+I_2^- + I_1^-I_2^+ - I_1^-I_2^-}{4i} \quad .$$

$I_1^+I_2^-$ and $I_1^-I_2^+$ are zero quantum coherence. $I_1^+I_2^+$ and $I_1^-I_2^-$ are double quantum coherence.

During the t_1 evolution under the B_0 gradient (The Hamiltonian is $\gamma\frac{dB_0}{dr} r I_z$), the zero quantum coherence evolves as the difference of the chemical shift frequencies of the two coupled spins. Two coupled nuclear spins are located near enough so that they experience the same magnetic field, i.e. the B_0 field causes no magnetic field difference on the coupled spins. The zero quantum coherence is therefore left unchanged,

$$(I_1^+I_2^- - I_1^-I_2^+) \rightarrow (I_1^+I_2^- - I_1^-I_2^+)e^{i\omega t}e^{-i\omega t} = (I_1^+I_2^- - I_1^-I_2^+) \quad .$$

The $90°_y$ pulse converts the zero quantum coherence into anti phased single quantum coherence, which will evolve into in-phased single quantum for detection purpose,

$$\frac{I_1^+I_2^- - I_1^-I_2^+}{4i} \rightarrow \frac{I_{1y}I_{2z} - I_{1z}I_{2y}}{2} \quad ,$$

All the non-zero quantum terms are dephased across the space. For example, the double quantum term,

$$(I_1^+I_2^+ + I_1^-I_2^-) \rightarrow (I_1^+I_2^+ e^{ig_z t_1} e^{ig_z t_1} - I_1^-I_2^- e^{-ig_z t_1} e^{-ig_z t_1}) = (I_1^+I_2^+ e^{i2g_z t_1} - I_1^-I_2^- e^{-i2g_z t_1}) \quad ,$$

where, $g_z = (\gamma \frac{dB_0}{dr} r)$ is spatially dependent across the space. The non-zero phase term in the double quantum coherence is averaged to zero. The discussion could be extended to triple, four and N-quantum coherence terms.

§5.4 Radio Frequency Gradient Zero Quantum Coherence Spectroscopy

When we design the RF gradient zero quantum coherence spectroscopy experiment, we need to pay attention to the characteristics common to RF gradient and B_0 gradient experiment.

(1) Only one gradient period should exist in the pulse sequence to avoid unexpected echo formation due to refocus of the phase of a coherence.

(2) The incremental time t_1 is applied after the 90°-Δ-180°-Δ–90° preparation pulse-delay train. This pulse-delay train creates multiple quantum coherence.

The RF gradient zero quantum coherence spectra experiment should also be fundamentally different from the B_0 gradient coherence spectra experiment.

(1) In B_0 gradient experiment, there is an overlap of t_1 and evolution period under B_0 gradient Hamiltonian. In RF gradient experiment, however, there is a separation of t_1 and the RF gradient evolution, for the phase encoding of the multiple quantum coherence can only happen during a z-quantized period. When the RF gradient is applied,

the spin system is requantized along RF gradient direction. In the RF gradient experiment, the t_1 interval occurs first, to introduce the multiple quantum coherence phase encoding, and then the RF gradient is applied to select the zero quantum coherence.

(2) In RF gradient experiment, an additional 90° pulse is required to facilitate the requantization of the spin system.

The RF gradient zero quantum coherence spectroscopy pulse sequence is shown in figure 5.3.

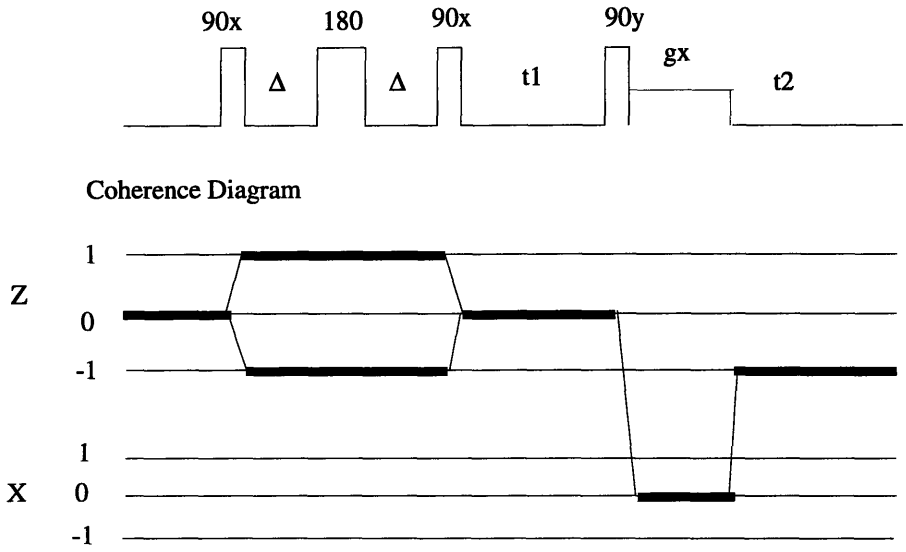

Figure 5.3 Pulse sequence and coherence diagram of the RF gradient zero quantum coherence spectroscopy.

The $90°_y$ pulse requantizes the ZQC, originally quantized along z direction, to ZQC along I_x direction without any loss, the RF gradient, g_x, destroys all the non-zero quantum coherence and allows the zero quantum coherence to pass through. A zero quantum coherence spectrum of 2 , 3-dibromopropionic acid was acquired on an AMX400 spectrometer. The spectrum is shown in figure 5.4.

§5.5 Radio Frequency Gradient Double Quantum Coherence Spectroscopy

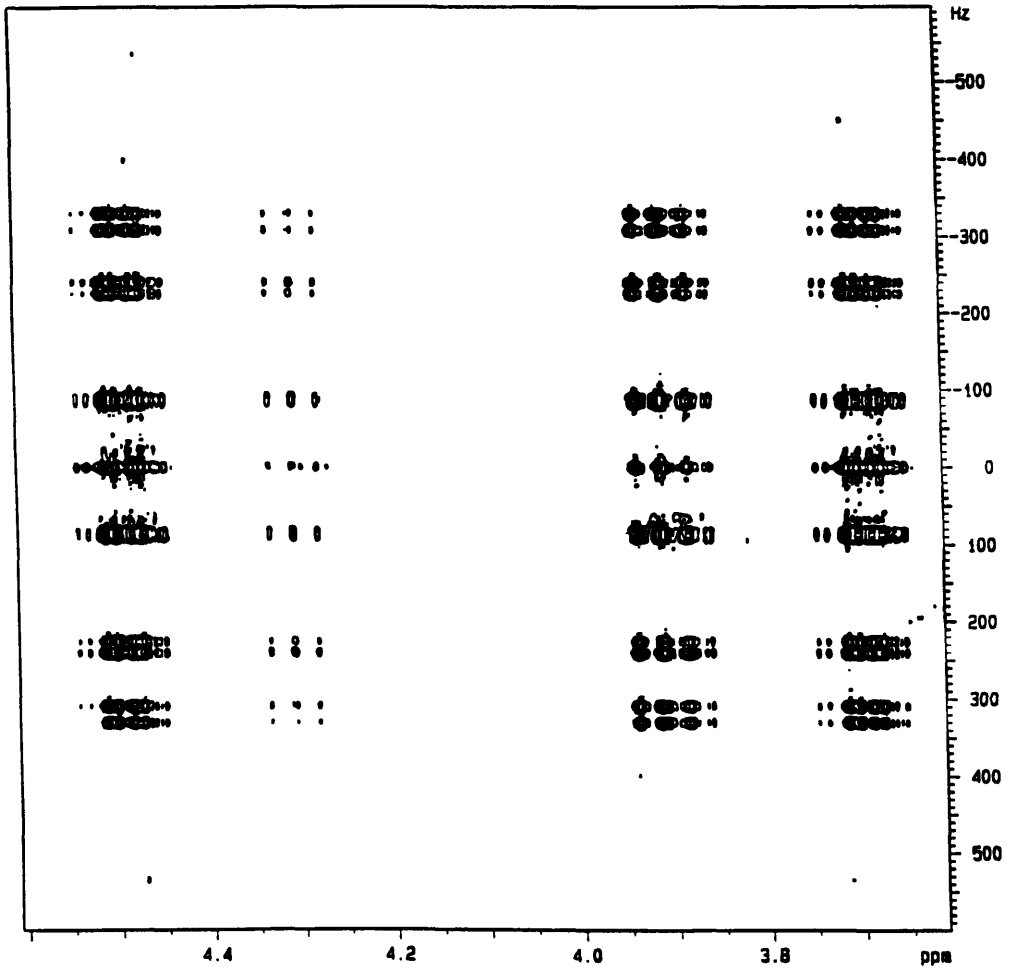

Figure 5.4 RF gradient zero quantum spectrum of 2,3-dibromopropionic acid on Bruker AMX 400., using pulse sequence of figure 5.3.

The design of the pulse sequence for an RF gradient multiple quantum coherence spectroscopy can be usefully compared to RF gradient multiple quantum filters. In an RF gradient double quantum filter COSY experiment, the spin state during incremental evolution period (t_1) is single quantum coherence, resulting in a 2D spectrum with single quantum coherence along both axes. In a double quantum coherence spectrum experiment, the evolution of multiple quantum

coherences are required during the incremental evolution period, t_1. One way of accomplishing this is to separate the two RF gradient pulses and allow the evolution to occur in between. In an RF gradient double quantum filtered COSY experiment, the first RF gradient pulse builds up multiple quantum coherence and starts with phase accumulation, and the second RF gradient refocuses the phase to allow echo formation prior to the detection period. During the first RF gradient period, the spin system is quantized along I_x, and a $90°_x$ pulse is inserted after the first RF gradient(x) to allow the spin system to requantize from z to I_x. Similarly, a second $90°_y$ pulse is inserted before the second RF gradient pulse to requantization spin system from z into the second RF gradient direction, I_x.

The pulse sequence and coherence diagram for the Radio Frequency Gradient Double Quantum Coherence Spectroscopy is shown in figure 5.5.

The $90°_x$-Δ-$180°$-Δ delay and pulse train prepares the spin system as antiphase single quantum coherence, then an RF gradient pulse is applied to requantize the spin system into a single quantum coherence along I_x direction. After the first radio frequency gradient, a $90°_x$ pulse is applied to requantize the spin system into double quantum coherence. The double quantum coherence will evolve a period of t_1. Then another 90° pulse is applied to requantize the spin system back to the I_x direction, spin system remains as a double quantum coherence, and a second radio frequency gradient is applied. This second gradient has only half of the time as the first gradient, but the spin system evolves twice as fast (a double quantum coherence evolves twice as fast as a single quantum coherence). Since the evolution of the spin system during the two gradient periods are of opposite directions, the phases exactly cancel each other. In other words, the phase is refocussed for the double quantum coherence. All of the other coherence orders are destroyed.

Two coherence pathways are selected, and they are originated from two different paths of gradient labeling.

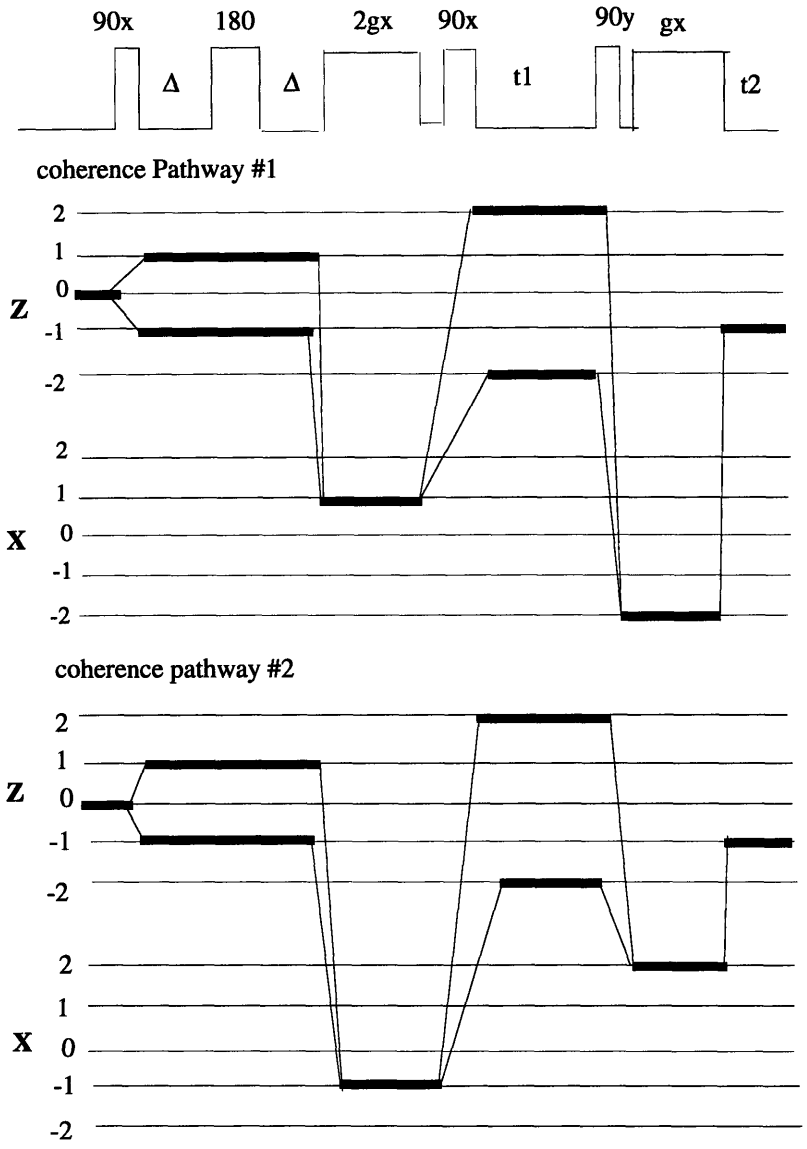

Figure 5.5 Pulse sequence and coherence diagram of the RF gradient double quantum coherence spectroscopy.

An interesting feature of the RF gradient experiments in this thesis is that they are phase sensitive experiments, since the spins of coherence number of both 2 and -2 are selected, a phase sensitive spectrum is achieved. However, for exactly the same reason, there is no quadrature detection in ω_1. In order to distinguish the positive

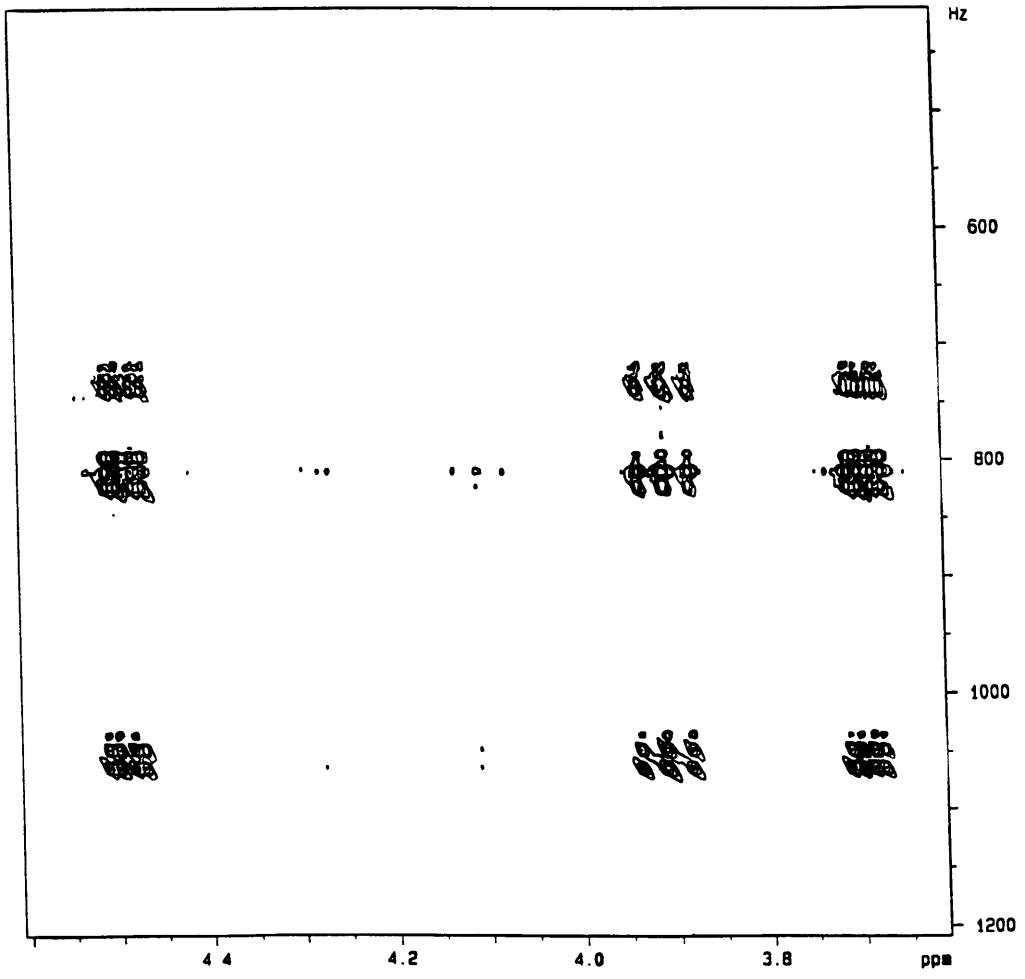

Figure 5.6 RF gradient double quantum coherence spectrum of 2,3-dibromopropionic acid on an AMX 400 spectrometer using pulse sequence of figure 5.5.

frequency and negative frequency relative to the reference frequency, spins of coherence number of either 2 or -2 (but not both) should be selected. In order to retain both features, TPPI (Time Proportional Phase Incrementation) should be included[5.2].

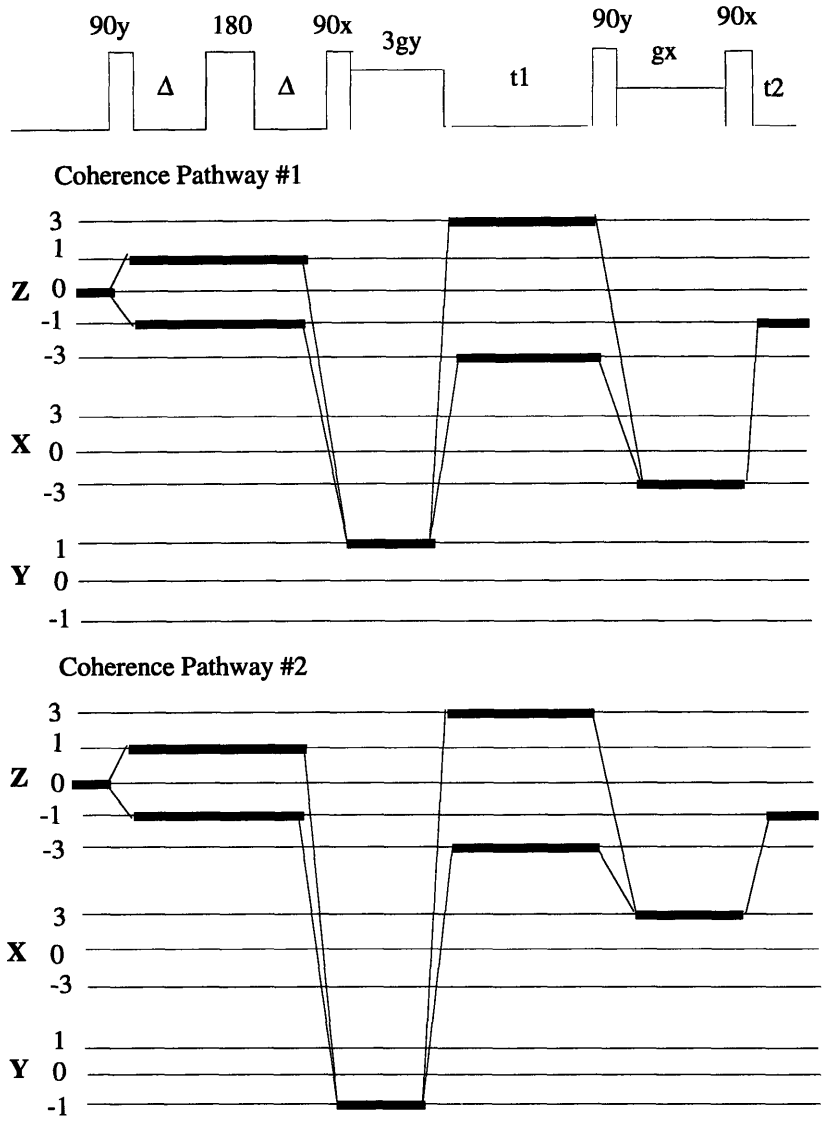

Figure 5.7 Pulse sequence and coherence diagram of the RF gradient triple quantum coherence spectroscopy.

The RF gradient double quantum coherence spectrum of 2 , 3-dibromopropionic acid was acquired on an AMX400 spectrometer. The spectrum is shown in figure 5.6.

§5.6 Radio Frequency Gradient Triple Quantum Coherence Spectroscopy

The pulse sequence for Radio Frequency Gradient Triple Quantum Coherence Spectroscopy is shown in figure 5.7.

The triple quantum coherence spectroscopy pulse sequence is very similar to that of the double quantum coherence spectroscopy. The desired triple quantum coherence are phase encoded during the t_1 evolution. They are requantized along I_y direction during the first radio frequency gradient duration, and evolve as single quantum coherences. They are requantized along I_x direction during the second radio frequency gradient where they evolve as triple quantum coherences and lead to a gradient echo. The last $90°_x$ pulse converts the desired coherence into z quantized single quantum for detection. All the rest of the coherence are dephased across the space and diminished from the signal. The product operator calculation gives the following overall result,

$$\frac{1}{8}\cos((\omega 1+\omega 2+\omega 3)t1)\,(I_{1y}I_{2z}I_{3z}+I_{1z}I_{2y}I_{3z}+I_{1z}I_{2z}I_{3y}) \quad .$$

The pulse sequence of the triple quantum coherence spectroscopy is typical of an N-quantum coherence spectroscopy, where N is an odd number. Higher quantum coherence pulse sequences need only the change of the two gradient ratio from 3:1 to N:1.

Similarly, the double quantum coherence spectroscopy is typical of any even number multiple quantum coherence spectroscopy. Higher quantum coherence pulse sequences need only the change of the gradient ratio from 2:1 to N:1.

§ 5.7 Radio Frequency Gradient Four Quantum Coherence Spectroscopy

The pulse sequence for the Radio Frequency Gradient Four Quantum Coherence Spectroscopy is shown in figure 5.8.

The product operator calculation gives the following overall result,

$$-\frac{3}{64}\cos((\omega 1+\omega 2+\omega 3+\omega 4)t1)\,(I_{1y}I_{2z}I_{3z}I_{4z}+I_{1z}I_{2y}I_{3z}I_{4z}+I_{1z}I_{2z}I_{3y}I_{4z}+I_{1z}I_{2z}I_{3z}I_{4y})\quad .$$

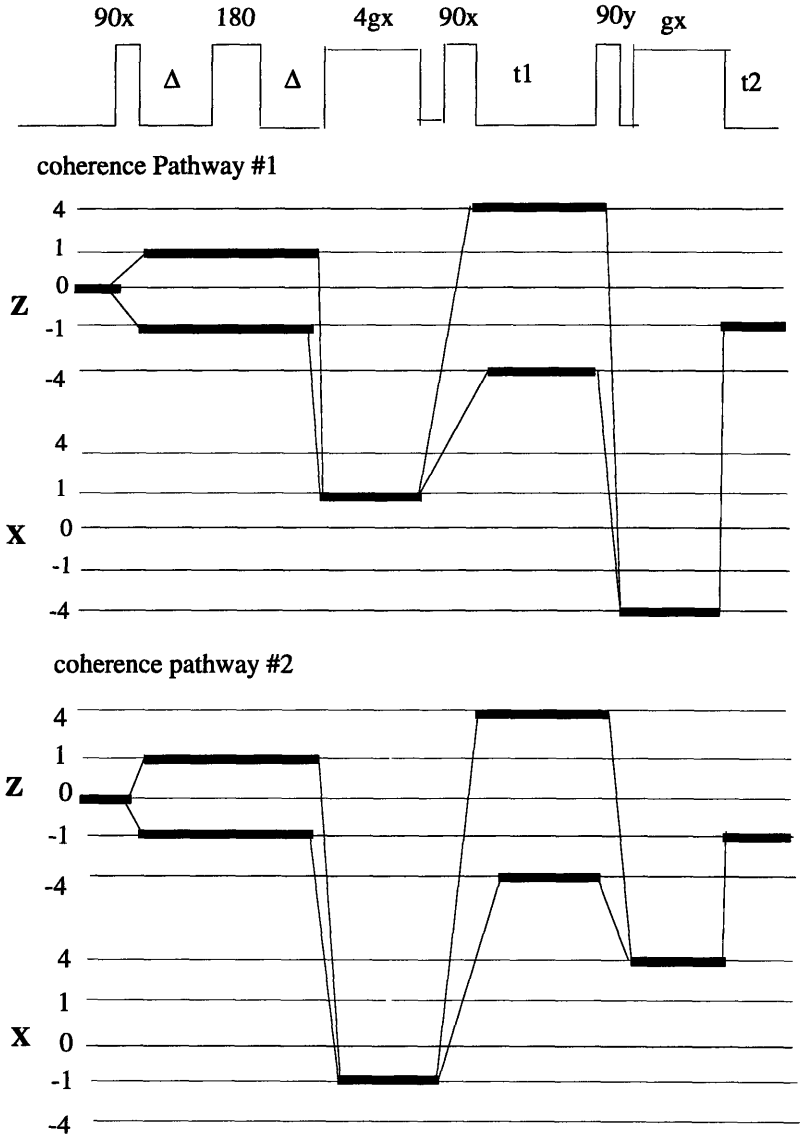

Figure 5.8 Pulse sequence and coherence diagram of the RF gradient four quantum coherence spectroscopy.

Chapter Six

Square Wave Modulation

§6.1 Sinusoidal Spatial Modulation vs. Square Wave Modulation

In a gradient experiment, the spin systems usually develop a sinusoidal modulation of the spin coherence across the sample. A brief analysis of RF gradient double quantum filter can help to illustrate this point.

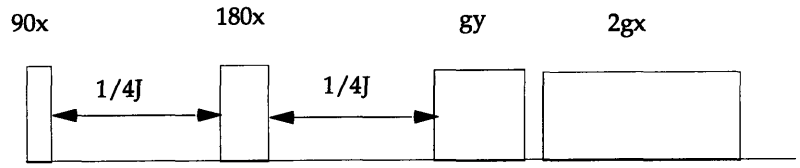

Figure 6.1 RF gradient double quantum filter pulse sequence

This pulse sequence was introduced in chapter two. The desired coherence pathway can be expressed, using Cartesian operator, as,

I_{1z}----$I_{1x}I_{2z}$----$I_{1x}I_{2z}$ $Cos^2(\theta)$----$I_{1x}I_{2z}$ $Cos^2(\theta)$ $Cos(2\theta)$,

where, $\theta = \theta(r) = \gamma \frac{\partial B_1}{\partial r} r\, t_g$ is spatial dependent, and t_g is the time of the gradient pulse. Since the signal is collected as the integrated value over the sample, spatial averaging is automatically achieved. The RF gradient is strong enough so that many cycles of θ are present across the sample and the end effects are not important, and it is valid to take the average of θ from 0 to 2π.

$$\int_0^{2\pi} \cos^2\theta \cos(2\theta)\, d\theta = \int_0^{2\pi} 0.5 \cos^2(2\theta)\, d\theta = \frac{1}{4} .$$

Notice that while the derived selectivity has been achieved, 3/4 of the signal is lost. The reason is that not all the spins throughout space

contribute fully to the signal. A sketch of function of $Cos^2(\theta)\ Cos(2\theta)$ clearly shows this as seen in figure 6.2.

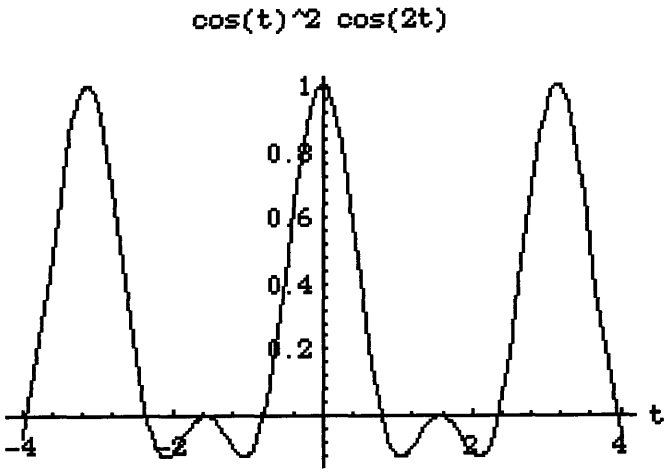

Figure 6.2 Plot of function, $Cos^2(\theta)\ Cos(2\theta)$

From figure 6.2, it is obvious that spins at only certain points contribute a maximum to the signal, and at some points, the spins contribute nothing. To increase the signal to noise ratio, a natural question is raised, is it possible to have all of the spins contribute a maximum to the signal? This will lead to the discussion of square wave modulation. Instead of exploring the square wave modulated pulse sequence directly, it is helpful to first introduce "nutation-angle-cycled" double quantum filter.

§6.2 Nutation-angle-cycled Double Quantum Filter

The importance of the nutation-angle-cycled double quantum filter(DQF) is that it can be transformed into an equivalent square wave modulated pulse sequence. The nutation-angle-cycled DQF pulse sequence is shown in figure 6.3. θ_1 and θ_1 are two orthogonal RF gradient pulses. For convenience, let's assume θ_1 is along y and θ_2 is along x.

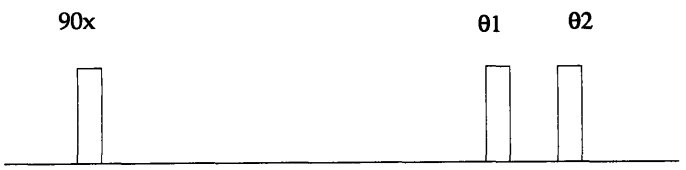

$\theta_1(y)$	0	$\pi/2$	π	$3\pi/2$
$\theta_2(x)$	0	π	0	π

Figure 6.3 Nutation-angle-cycled double quantum filter pulse sequence.

The pulse sequence of the nutation-angle-cycled DQF is a hybrid of the phase cycled DQF and the RF gradient DQF. Like the phase cycled DQF pulse sequence, the nutation-angle-cycled DQF takes four scans of varied pulse sequences to select the desired coherence pathway and to destroy the undesired coherence pathways. The difference between the two is that the nutation angles, not the phases of the pulse sequence, are varied. On the other hand, the nutation-angle-cycled DQF pulse sequence is similar to the RF gradient pulse sequence, since in the position of the two orthogonal RF gradients, there are now two pulses, θ_1 and θ_2 with varying nutation angles. These two pulse lengths are cycled through four scans instead of being averaged over space in a gradient experiment.

The first 90° pulse excites the spin system, and following the t_1 evolution period the coupled spins develop anti-phase magnetization. At the end of the t_1 evolution period, there are four spin states, I_{1x}, I_{1y}, $I_{1x}I_{2z}$, $I_{1y}I_{2z}$. The last two nutation-angle-cycled pulses choose the coupled spin system. The desired coherence pathway is the following,

$I_{1x}I_{2z}$ -> $I_{1x}I_{2z}\cos^2(\theta 1)$ - $I_{1z}I_{2x}\sin^2(\theta 1)$
-> $I_{1x}I_{2z}\cos^2(\theta 1)\cos(\theta 2)$ - $I_{1z}I_{2x}\sin^2(\theta 1)\cos(\theta 2)$
-> $2(I_{1x}I_{2z} + I_{1z}I_{2x})$

The nutation-angle-cycled DQF has the same sensitivity as the phase cycled experiment. During the four scans, the nutation angles, instead of the phases of the pulses, change. One question is weather it is possible to achieve the same sensitivity with only one pulse sequence.

§6.3 Square Wave Modulated Double Quantum Filter

In the nutation-angle-cycled double quantum filter pulse sequence (figure 6.3). each $\theta_1(y)$ pulse can be decomposed into three pulses and $\theta_2(x)$ pulse into 2 pulses. After replacing the old pulses ($\theta_1(y)$ and $\theta_2(x)$) with the new pulse trains, we get a new nutation-angle-cycled DQF pulse sequence, where each scan consists of 6 pulses, instead of 4 pulses.

$90°_x$ --(t_1)-- $135°_y$ ---- $-90°_y$ ---- $-45°_y$ ---- $90°_x$ ---- $-90°_x$
$90°_x$ --(t_1)-- $135°_y$ ---- $-90°_y$ ---- $45°_y$ ---- $90°_x$ ---- $90°_x$
$90°_x$ --(t_1)-- $135°_y$ ---- $90°_y$ ---- $-45°_y$ ---- $90°_x$ ---- $-90°_x$
$90°_x$ --(t_1)-- $135°_y$ ---- $90°_y$ ---- $45°_y$ ---- $90°_x$ ---- $90°_x$

A closer look at the pulse sequence across the scans will help to show that there are simple periodic patterns across the scans. The third pulses cycled through the pattern of ($-90°_y$, $-90°_y$, $90°_y$, $90°_y$), the fourth pulses cycled through the pattern of ($-45°_y$, $45°_y$, $-45°_y$, $45°_y$), and the last pulses cycled through the pattern of ($-90°_x$, $90°_x$, $-90°_x$, $90°_x$). These three patterns have some similarities.

1 In the same pattern, there is a single nutation axis through the cycles. The third, fourth, the fifth pulses have nutation axes of I_y, I_y, I_x, respectively.

2 In the same pattern, there is a single nutation angle (in the sense of absolute value) throughout the cycles. The Third, fourth, and fifth pulses have nutation angle of 90°, 45°, 90°, respectively.

3 In the same pattern, the sign of the nutation angles change periodically across the cycle. The period of the phase change of the third pulse is twice as long as that of the fourth pulse and fifth pulse.

§6.4 Square Wave Modulated Pulse Design

The design of the SWM(θ_{axis}, l) pulse is such that the time series of the pulse train excites the spin system so that the magnetization will have a square wave modulated pattern throughout the space. The problem is simplified to a mapping from the time domain (time series of pulse train) to the spatial domain (the spin alignment across space). Finally, the Bloch equations are used to analyze the pulse sequence, and to verify the spin spatial arrangement.

In order to map from the pulse sequence in the time domain to the spin alignment in the spatial domain, we recall that the frequency and the spatial domains are linearly related, with the proportionality constant being the gradient strength.

While the Bloch equations do not, in general, follow a simple Fourier picture, if the RF field is applied on resonance and the gradients are limited to be between RF pulses, the Fourier relation between the frequency and time domains provides a correct picture of the excitation profile. The inverse transform of the spin excitation profile in the frequency domain can suggest the time pattern of the RF excitation pulse sequence. We will use this to build up a sequence of square wave modulation pulses.

Let's start with the first mapping. As we have discussed before, the Fourier transform of the pulse sequence in the time domain will approximately give the spin excitation profile in the frequency domain. An inverse transform of the spin excitation profile in the frequency domain can suggest the possible time pattern of the RF excitation pulse sequence. The inverse Fourier transform of the square wave will give rise to the anti symmetric modulation:

1. Square wave modulated spin profile is shown in figure 6.4.

2. Inverse Fourier transform of the square wave function, i.e. -2 $\sin^2(\pi t)/t$, is shown in figure 6.5.

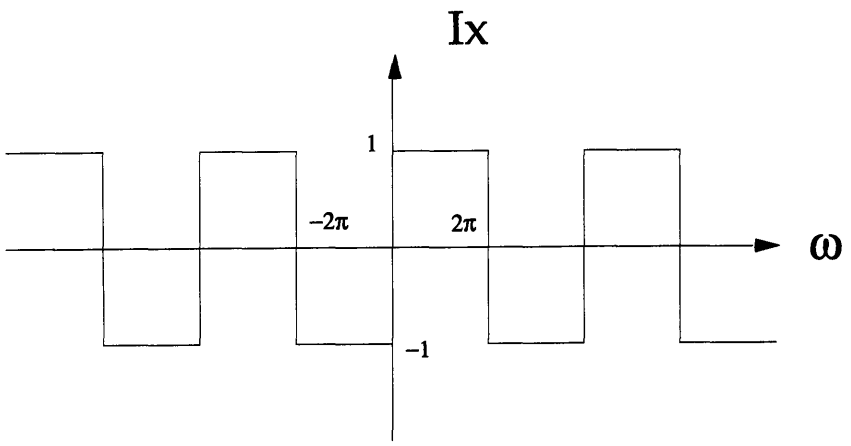

Figure 6.4 Square wave modulated spin profile.

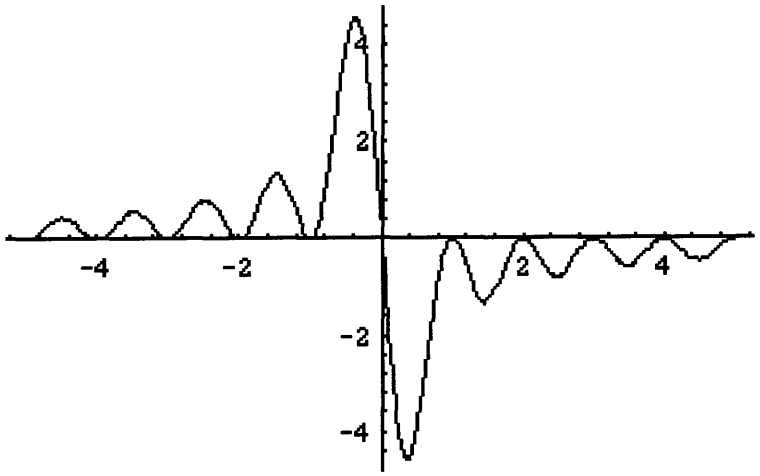

Figure 6.5 Inverse Fourier transform of the square wave function.

In order to keep the linear dynamics, the sequence is transformed to the set of gradient pulses shown in figure 6.6.

An intuitive convolution analysis can help to demonstrate this solution. The desired frequency domain excitation profile is the convolution of three functions, a top-hat function, two delta functions (180° out of phase), and a comb function. The decomposition of the frequency domain excitation profile is illustrated in figure 6.7, 6.8, 6.9.

Figure 6.7 is the tophat function, figure 6.8 is double delta functions, and figure 6.9 is a comb function.

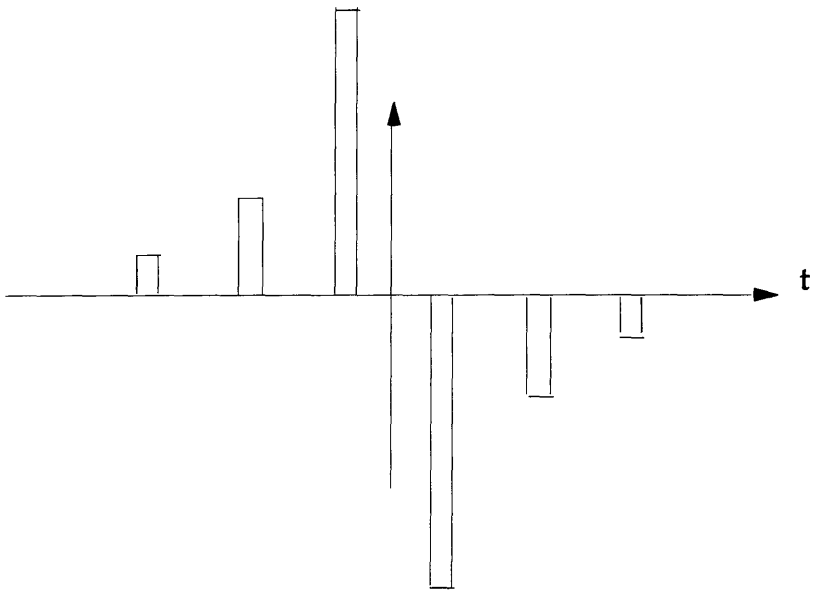

Figure 6.6 Discrete approximation of figure 6.5.

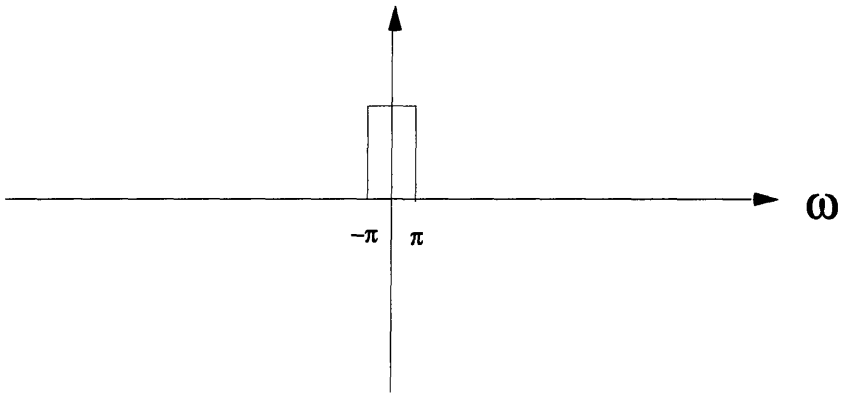

Figure 6.7 Top hat function.

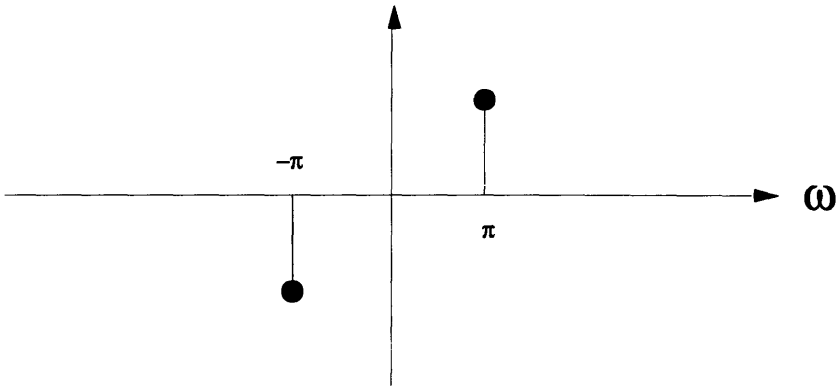

Figure 6.8 Double delta function.

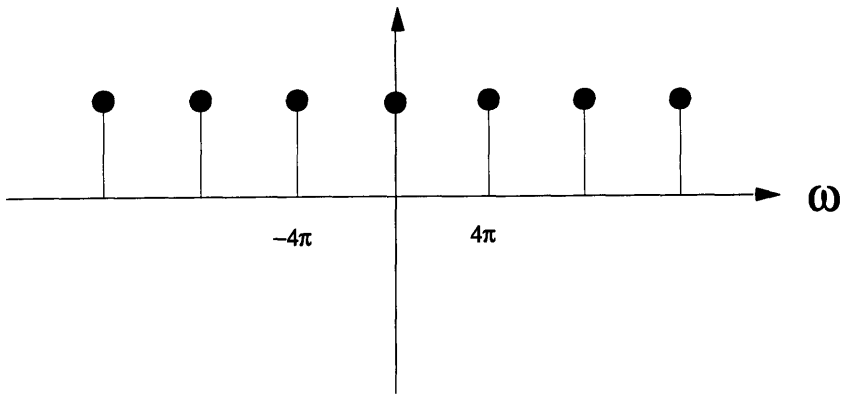

Figure 6.9 Comb function.

The convolution theorem in Fourier analysis states that if we convolute two signals in the time domain, this is equivalent to multiplying their spectra in the frequency domain. The time domain equivalents of the three functions that make up the square wave modulation are a Sinc function(figure 6.10), a sine function(figure 6.11), and a comb function(figure 6.12). The product of these is the desired time-domain RF excitation pattern.

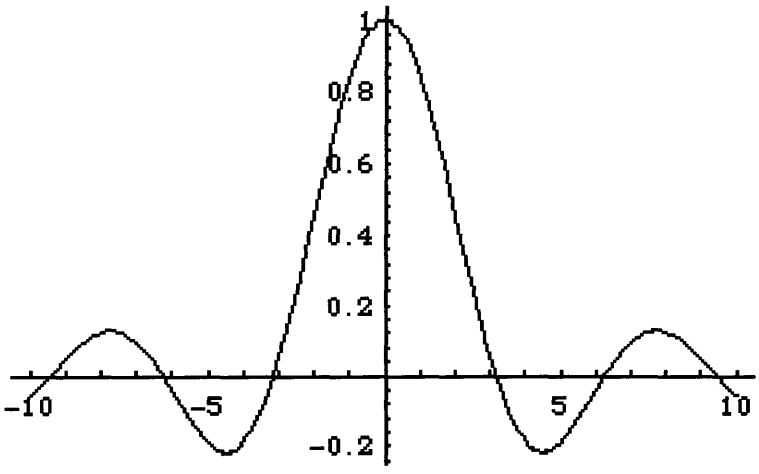

Figure 6.10 Sinc function.

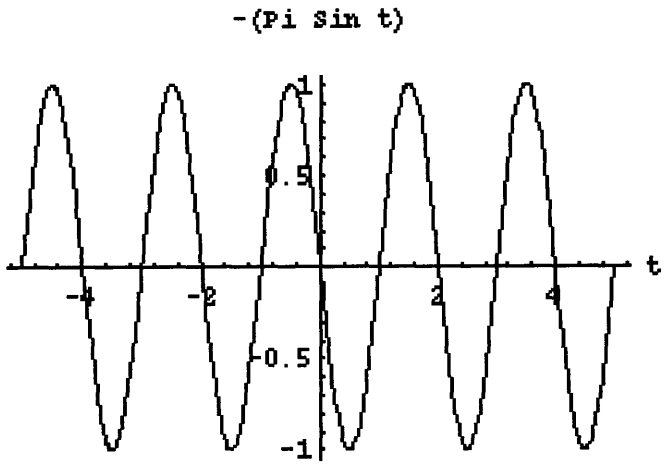

Figure 6.11 Sine function.

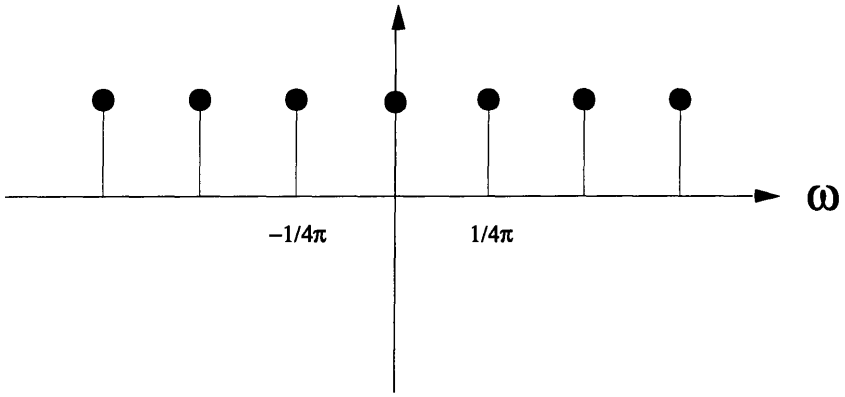

Figure 6.12 Comb function.

Now let's look at the mapping from the spin excitation profile in the frequency domain to the spin alignments in the space domain. These two domains are related by the gradient imposed frequency shift,

$$\Delta\omega = \gamma \frac{dB_0}{dr} r \ ,$$

where r is the spatial unit along the axis of linear gradient. It is obvious that the mapping from the spin excitation profile in the frequency domain to the spin excitation profile in space domain is linear.

There are two possible ways of combining B_0 gradients with RF pulses, one way is to allow the gradient to be on during the whole

pulse sequence. This approach has a problem, since when the RF pulse and the B_0 gradient overlapped, an off-resonance term is introduced, and the effective field is tilted away from the transverse plane. The nutation around this axis leads to errors. In the square wave modulation experiment, the effectiveness of the pulse sequence depends on the exactness of every pulse (its intensity, phase, etc.), and this off-resonance term will create a fatal problem.

A better approach is to apply the B_0 gradient only between the RF pulses so that the gradient is off during the RF pulses.

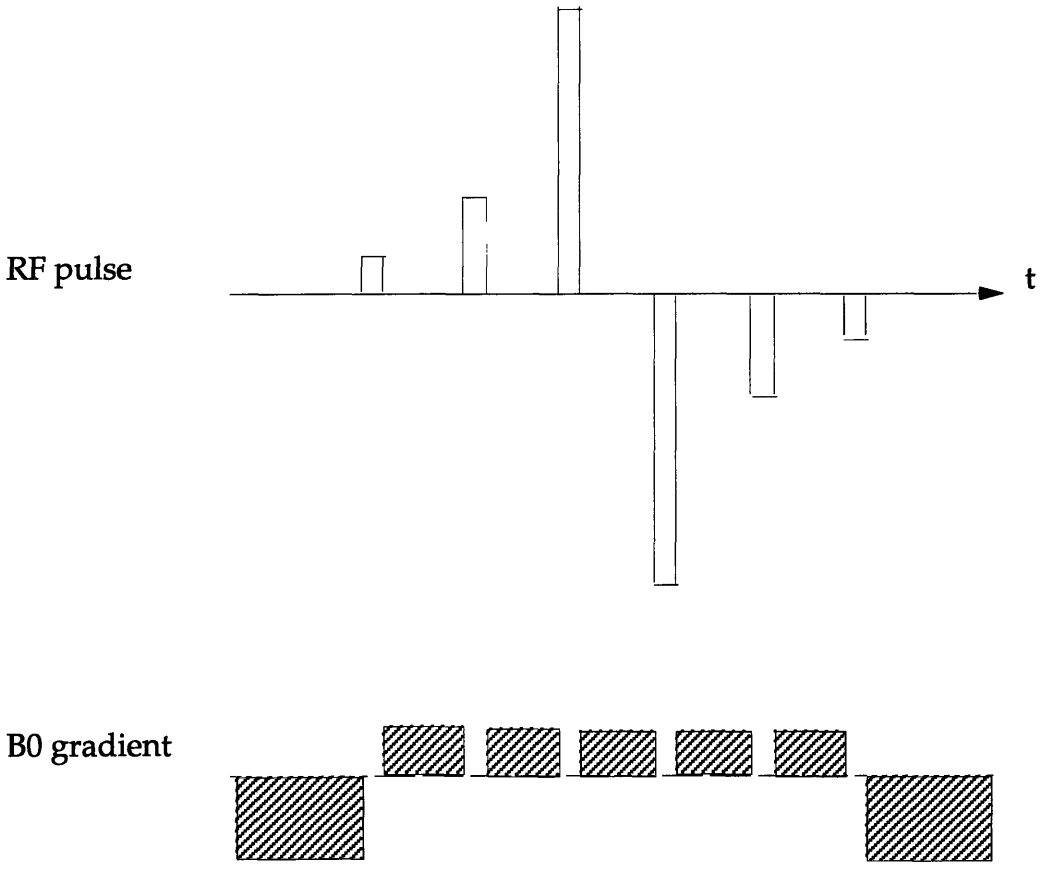

Figure 6.13 Pulse sequence that achieves spatial square wave modulation. The pulse sequence is (-2.5$B_0(\Delta\omega)$) -- (1/5)θ -- $B_0(\Delta\omega)$ -- (1/3)θ -- $B_0(\Delta\omega)$ -- θ -- $B_0(\Delta\omega)$ -- (-θ) -- $B_0(\Delta\omega)$ -- (-1/3)θ -- $B_0(\Delta\omega)$ -- (-1/5)θ -- (-2.5$B_0(\Delta\omega)$), where $\Delta\omega = \gamma \frac{dB_0}{dr} r$, and θ is the homogeneous nutation angle across the space.

The final composite RF and B_0 gradient pulse sequence is shown in figure 6.13.

Since it is necessary to introduce the B_0 gradient evolution to map from the spin excitation profile in the Frequency domain to the spin excitation profile in the space domain, there is additional complication accompanying B_0 gradient. The spins have spatial dependent phase shift due to the gradient evolution. The phase shifts must be twisted back to create a gradient echo. The first and the last B_0 gradients are used to refocus the phase dispersions among the spins of different spatial location. The sum of the areas under these two gradient strength curve(vs. time) are the same as the sum of the area under the curves of the five B_0 gradient in the middle. This is just like a gradient echo.

§6.5 Bloch Equations and Rotation Matrix Analysis

In the absence of spin-spin couplings, the spin dynamics can be studied with the Bloch equation. Now, we consider a case of single spin (no J coupling), so that the Bloch equation is a full description of the spin dynamics. We can solve the Bloch equation as an ordinary differential equation to analyze the spin dynamics under the influence of RF pulse and B_0 gradient. The Bloch equation in the rotating frame is stated as the following:

$$dM_x/dt = \gamma (M_y B_z - M_z B_y) - M_x/T_2$$
$$dM_y/dt = \gamma (M_z B_x - M_x B_z) - M_y/T_2$$
$$dM_z/dt = \gamma (M_x B_y - M_y B_x) - (M_z - M_0)/T_1$$

It is useful to use a solution to the Bloch equations for the purpose of explanation of the frequency spectrum of these pulses.

1. The spin is on resonance when the RF is turned on and the B_0 gradient is turned off. So during RF pulse, the magnetization is nutated along an axis in the rotating frame, say I_x. Since the pulse duration is only on the order of microsecond, the excitation profile in the

frequency domain is flat over the chemical shift range of the experiment.

2. The relaxation time T_1 and T_2 are long compared with the composite pulse sequence so that the relaxation terms in the Bloch equation vanish. This is a very reasonable assumptions. In the case of water sample, the relaxation time is on the order of seconds and the time scale of the square wave modulated pulse sequence is on the order of milliseconds.

With these two assumptions, we can rewrite the Bloch equations as the following.

During the RF pulse (we have assumed the pulse is along Ix) nutation period, there is only RF term on the right hand side of the Bloch equation:

$$dM_x/dt = 0$$
$$dM_y/dt = \gamma M_z B_x = \Delta\omega_1 M_z$$
$$dM_z/dt = -\gamma M_y B_x = -\Delta\omega_1 M_y$$

where $\Delta\omega_1$ is the nutation frequency, $\Delta\omega_1 = \gamma B_1$, which is homogeneous across the sample space. If we assume that the strength of the RF pulse is the same, the duration of the pulse can be determined through: $t_p = \phi/\Delta\omega_1 = \phi/(\gamma B_1)$. where ϕ is the required nutation angle of each of the RF pulses. ϕ is equal to $(1/5)\theta$, $(1/3)\theta$, θ, $-\theta$, $(-1/3)\theta$, $(-1/5)\theta$, respectively. θ is the universal nutation angle for all the spins after the composite pulse sequence.

During the B_0 gradient evolution period, the right-hand side of the Bloch equation consists of only B_0 gradient induced off-set evolution terms. The Bloch equation is as the following:

$$dM_x/dt = \gamma M_y B_z = \Delta\omega M_y$$
$$dM_y/dt = -\gamma M_x B_z = -\Delta\omega M_x$$
$$dM_z/dt = 0 \quad ,$$

where $\Delta\omega = \gamma \frac{\partial B_0}{\partial x} x$. $\Delta\omega$ is a spatial dependent offset term.

Now, we can solve the problem in three equivalent ways.

(1) Numerically solve the Bloch equation, which is an ordinary differential equation.

(2) Analytically solve the Bloch equation.

(3) Rotation matrix calculation.

With the first two methods, the initial condition for the magnetization ($M_x(0)$, $M_y(0)$, $M_z(0)$) is used to solve the first Bloch equation, i.e. the nutation under the RF pulse. The state of the magnetization is calculated at the end of the nutation, i.e. at time equals t_{p1}. This state of magnetization ($Mx(t_{p1})$, $My(t_{p1})$, $Mz(t_{p1})$) is carried forward to be the initial condition for the next Bloch equation set, i.e. the precession under B_0 gradient. A new state of magnetization ($M_x(t_{p1}+\tau)$, $M_y(t_{p1}+\tau)$, $M_z(t_{p1}+\tau)$) is calculated from solving this second set of Bloch equation. The two Bloch equation sets (one for the RF pulse nutation period and the other for the B_0 gradient precession period) will be solved alternatively and repetitively just to follow the course of the train of RF pulse and B_0 gradient sequence to get the final solution, i.e. the final state of the magnetization.

Rotation matrix calculation is an equivalent way of solving the Bloch equation in case of neglecting the T_1 and T_2 relaxation (in case of long relaxation time). In our case the spin is on resonance, so the evolution will take the form of rotation of magnetization along x axis during the RF pulse nutation period, and along z axis during B_0 gradient precession period. In a more general case including off-resonance spin dynamics, the spin magnetization will rotate along a certain axis in the space in the rotating frame, which is determined by

the RF gradient strength and the B_0 residue along the Z due to off-resonance. The rotation matrices are defined as the following.

1. Rotation around x axis.

$$\text{RotMatx}(t) = \begin{bmatrix} 1 & 0 & 0 \\ 0 & \cos(t) & -\sin(t) \\ 0 & \sin(t) & \cos(t) \end{bmatrix}$$

2. Rotation around y axis.

$$\text{RotMaty}(t) = \begin{bmatrix} \cos(t) & 0 & \sin(t) \\ 0 & 1 & 0 \\ -\sin(t) & 0 & \cos(t) \end{bmatrix}$$

3. Rotation around z axis.

$$\text{RotMatz}(t) = \begin{bmatrix} \cos(t) & -\sin(t) & 0 \\ \sin(t) & \cos(t) & 0 \\ 0 & 0 & 1 \end{bmatrix}$$

The solution then reduces to matrix multiplication. Assuming the following:

1. The universal nutation angle across the sample is θ.

2. The spatial dependent frequency component is ω.

3. The magnetization is initially along z axis, i.e. {0, 0, 1}.

If we define the final state of a square wave modulated Y pulse $SWM(\theta_y, 1)$ as echo[θ,ω(l)], we will have:

```
echo[θ_,ω_]:=        RotMatz[-2.5 ω] . RotMatx[θ/5] . RotMatz[ω] \
      . RotMatx[θ/3] . RotMatz[ω] . RotMatx[θ] . RotMatz[ω] \
      . RotMatx[-θ] . RotMatz[ω] . RotMatx[-θ/3] . RotMatz[ω] \
      . RotMatx[-θ/5] . {0,0,1}
```

Similarly, the square wave modulated X pulse SWM(θ_X, l) can be calculated through:

```
echo[θ_,ω_]:=  RotMatz[-2.5 ω] . RotMaty[-θ/5] . RotMatz[ω] \
        . RotMaty[-θ/3] . RotMatz[ω] . RotMaty[-θ] . RotMatz[ω] \
        . RotMaty[θ] . RotMatz[ω] . RotMaty[θ/3] . RotMatz[ω] \
        . RotMaty[θ/5] . {0,0,1}
```

θ is adjusted to be $\pi/3$, which gives the best square wave modulated pattern.

A calculation of the spin magnetization after the SWM(90°x,l) is given below:

(1) The initial spin magnetization is along Z. After the SWM(90°x,l), it should be along +/- Y with square wave modulated pattern.

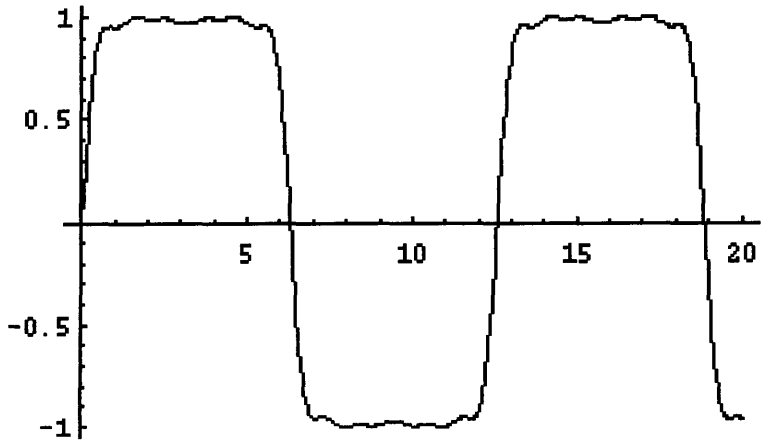

Figure 6.14 Initial magnetization was along Z. After spatial square wave modulated 90x pulse, the magnetization lay along +/- Y.

(2) The initial spin magnetization is along Y. After the SWM(90°x,l), it should be along +/- Z with square wave modulated pattern.

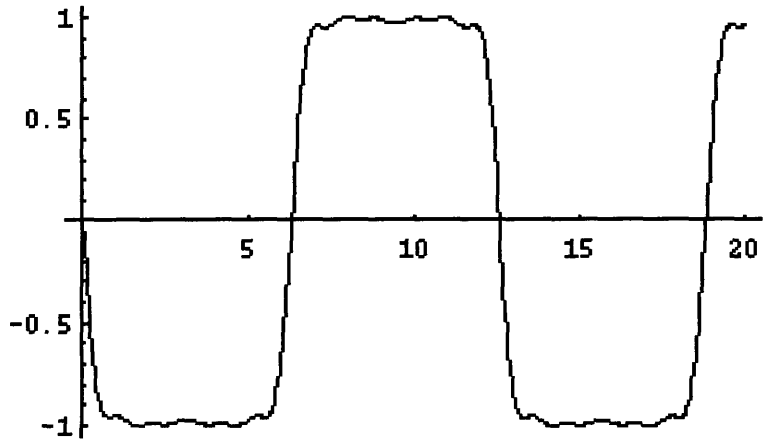

Figure 6.15 Initial magnetization was along Y. After spatial square wave modulated 90x pulse, the magnetization lay along +/- Z.

(3) The initial spin magnetization is along X. After the SWM(90°x,l), the spin is locked along X.

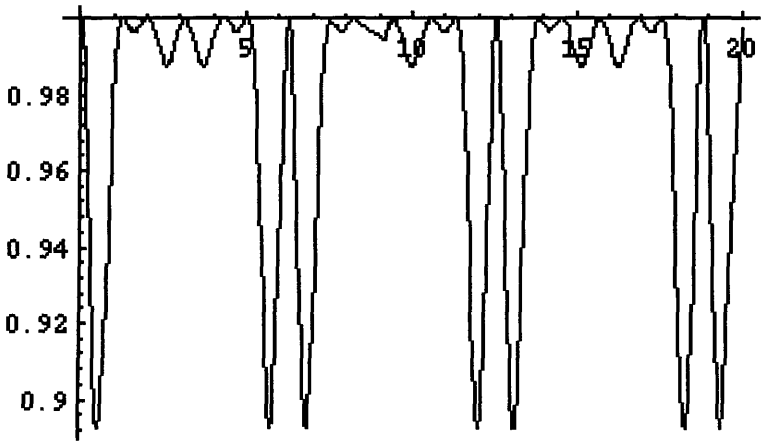

Figure 6.16 Initial magnetization was along X. After spatial square wave modulated 90x pulse, the magnetization was spin locked along X.

A calculation of the spin magnetization after the SWM(90°y,l) is given below:

(1) The initial spin magnetization is along Z. After the SWM(90°y,l), it should be along +/- X with square wave modulated pattern.

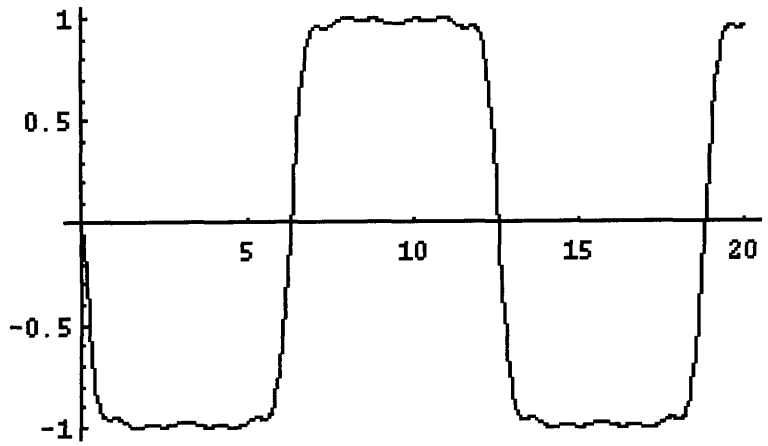

Figure 6.17 Initial magnetization was along Z. After spatial square wave modulated 90y pulse, the magnetization lay along +/- X.

(2) The initial spin magnetization is along X. After the SWM(90°y,l), it should be along +/- Z with square wave modulated pattern.

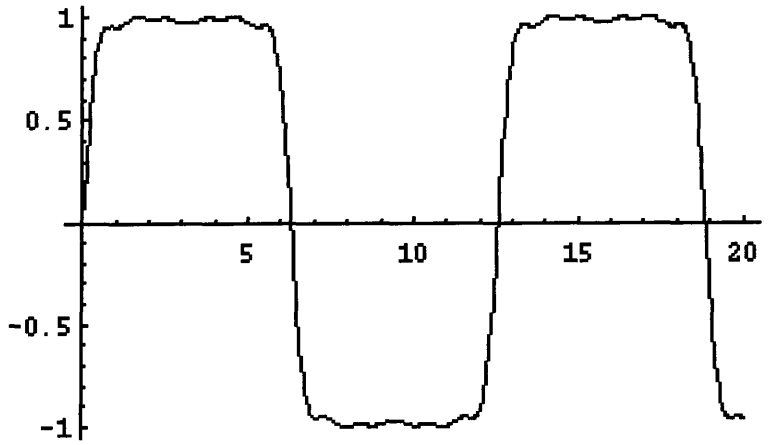

Figure 6.18 Initial magnetization was along X. After spatial square wave modulated 90y pulse, the magnetization lay along +/- Z.

(3) The initial spin magnetization is along Y. After the SWM(90°y,l), the spin is locked along Y.

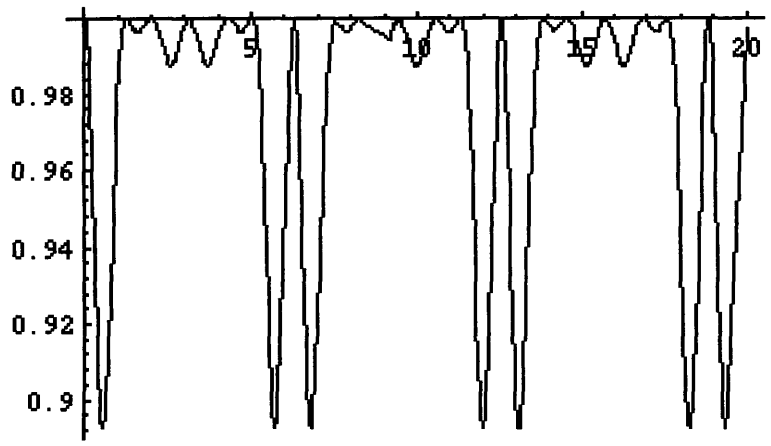

Figure 6.19 Initial magnetization was along Y. After spatial square wave modulated 90y pulse, the magnetization was spin locked along Y.

A calculation of the spin magnetization after the SWM(90°z,l) is given below:

(1) The initial spin magnetization is along Y. After the SWM(90°z,l), it should be along +/- X with square wave modulated pattern.

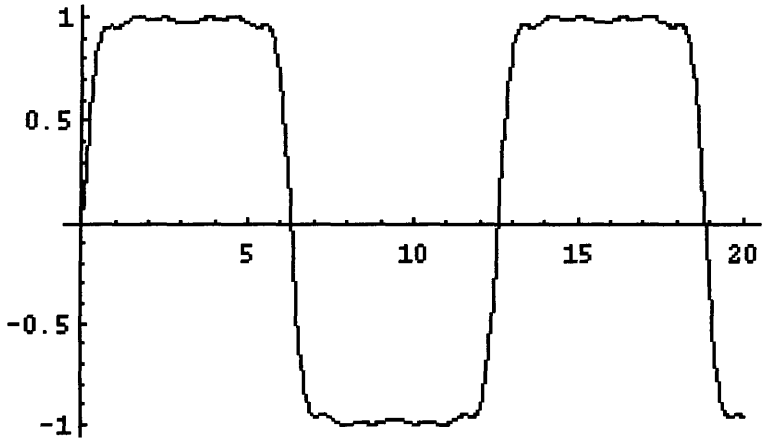

Figure 6.20 Initial magnetization was along Y. After spatial square wave modulated 90z pulse, the magnetization lay along +/- X.

(2) The initial spin magnetization is along X. After the SWM(90°z,l), it should be along +/- Y with square wave modulated pattern.

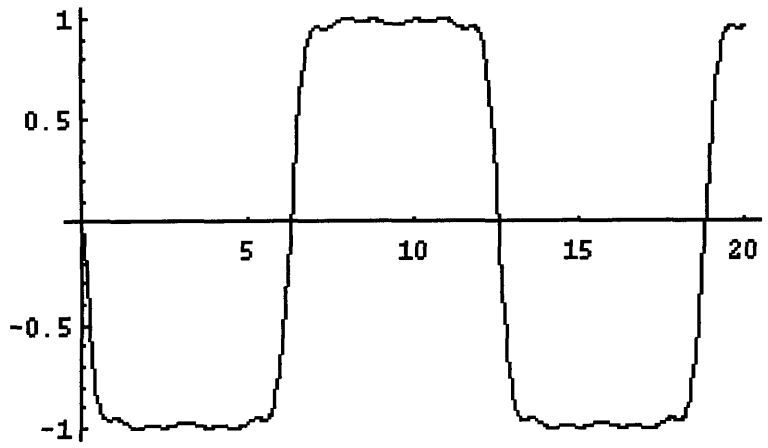

Figure 6.21 Initial magnetization was along X. After spatial square wave modulated 90z pulse, the magnetization lay along +/- Y.

(3) The initial spin magnetization is along Z. After the SWM(90°z,l), the spin is locked along Z.

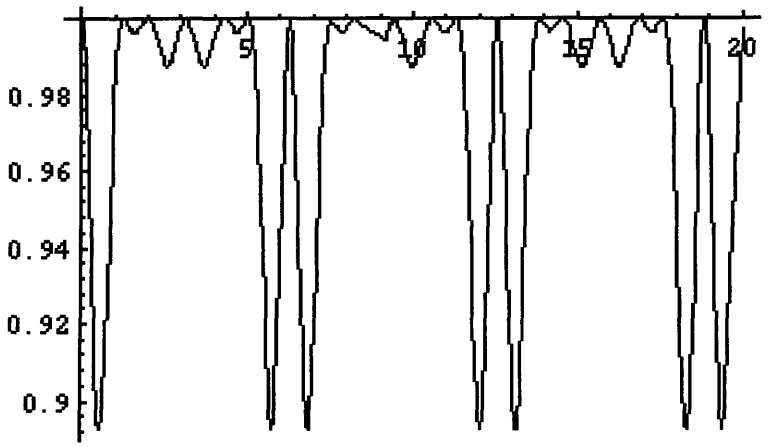

Figure 6.22 Initial magnetization was along Z. After spatial square wave modulated 90z pulse, the magnetization was spin locked along Z.

The implementation of the SWM(90°z,l) is a little bit different from the SWM(90°x,l) and SWM(90°y,l). Now, the RF pulse is replaced by composite Z pulse, and the B_0 gradient is replaced by RF gradient.

From the studies of the square wave modulated pulse sequences , the followings are found to be important:

(1) When the B_0 gradient effective area(the area under the curve of the B_0 gradient vs. time) is doubled, the spin spatial modulation frequency will be doubled or the periodicity will be reduced by half.

(2) When the RF pulse effective area(the area under the curve of the RF pulse) is doubled, the spatial nutation angle will be doubled.

§ 6.6 Experimental Results

Figure 6.23 is the square wave modulated spectrum of water acquired on the Bruker AMX400 spectrometer. Figure 6.24 is another spectrum with twice the spatial modulation frequency.

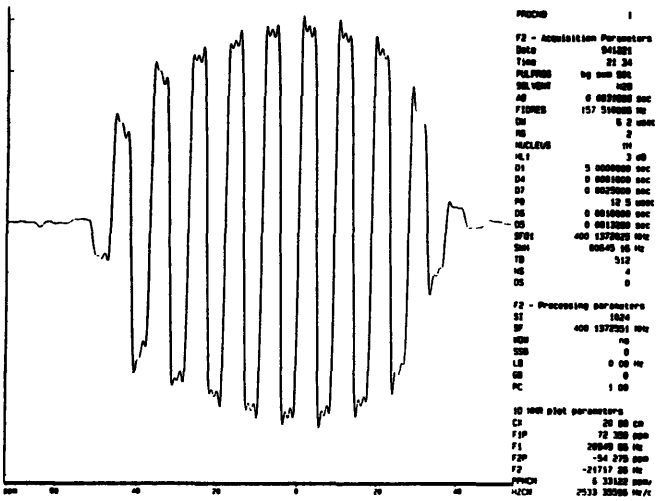

Figure 6.23 Square wave modulated spectrum of water acquired on Bruker AMX 400 spectrometer.

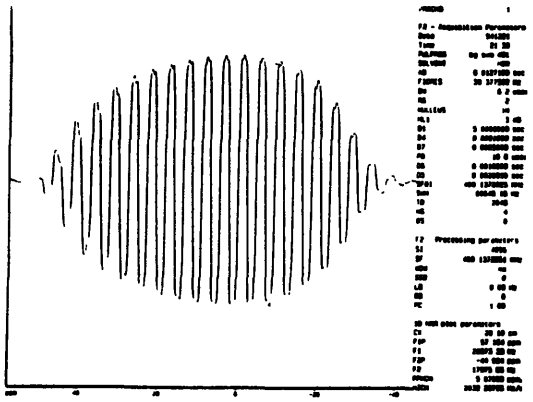

Figure 6.24 Square wave modulated spectrum of water acquired on Bruker AMX 400 spectrometer.

Chapter Seven

Conclusions

High resolution, multi-dimensional, solution state NMR spectroscopy is a unique method to study the structure, dynamics, and reactions of large and small molecules, which in turn, provide keys to understand their functions and properties. In these work, we have furthered the development of NMR methodologies suitable for the study of biomolecules, and in particular, we have attempted to advance the issue of selectivity, limited dynamic range, and sensitivity.

Gradient enhanced multiple quantum filters have been designed that eliminate the undesired strong solvent peak(single quantum) without incurring dynamic range problems. RF gradient experiments have many potential advantages over B_0 gradient methods. They are more convenient and permit flexible manipulation of the spin magnetization. In heteronuclear experiments, the RF gradient only affects the proton spins and gradient can be oriented along any direction in the transverse plane. The RF gradient field is non-secular, and therefore RF gradients can average out internal interactions and hence interrupt spin evolution save that from the gradient itself. In the presence of an RF gradient, the effective relaxation time is longer.

RF gradient fields which simultaneously induce coherence transformations and impose a spatially dependent phase shift on a spin system can be used to implement simple and efficient multiple quantum filters. In this thesis, a new methodology is presented that facilitates the design and understanding of NMR experiments in which RF gradients are used. The spin states are expressed in a frame aligned with the rotating frame axis of the RF gradient and to each spin state is assigned a new set of effective coherence numbers, corresponding to the relative rate of evolution in the RF gradient field. This re-quantization procedure allows the conceptual separation of the coherence transformation, induced by the RF gradient, and the gradient evolution.

In the original sense, a multiple quantum filter involves a z-quantized multiple quantum state. Since the spin system is always z-quantized, such a definition of a multiple quantum filter is a natural choice. But such a definition makes it very difficult to analyze an RF gradient multiple quantum filter, where, for instance, the selected spin system may never pass through a z-quantized multiple quantum state. In this paper, the three quantization axes are equivalent in importance. The spin system is quantized along z axis when there are no RF gradients. During an RF gradient pulse, the spin system is quantized along the direction of the RF gradient field. The generalized concept of an multiple quantum filter is to select that subset of spins that are involved in couplings with a given number of other spins. After introducing the requantization methodology, several generalized RF gradient multiple quantum filters were designed and analyzed. The sensitivity of the two most conveniently designed RF gradient multiple quantum filters were analyzed and compared.

In addition to RF gradient multiple quantum filters, general RF gradient multiple quantum coherence spectrum experiments were designed including zero, two, three, four quantum coherence spectrum experiments. The pulse sequence for the higher multiple quantum coherence spectrum experiments can be obtained through the double quantum coherence spectrum (for the even quantum coherence spectrum), or triple quantum coherence spectrum (for the odd quantum coherence spectrum).

Square wave modulation was explored as a means of enhancing the sensitivity of gradient experiments. When gradients are used to select coherence pathways, the spatial distribution of the spin state is usually sinusoidally modulated so that spins at many locations only contribute partially to the signal intensity. The motivation of square wave modulation is to allow every spin to contribute the maximum amount to the final signal intensity. In our analysis, a square wave modulated pulse consists of a train of RF pulses and B_0 gradients. The design of such a pulse and gradient train has focused on two particular

mappings, derived from a Fourier analysis of the spin excitation profile. These were verified by Bloch equations. Simulations have shown to yield the expected gains in signal-to-noise ratio.

The methods developed in this thesis have direct applications to modern high resolution NMR studies of large biomolecules. The theoretical description of spin dynamics in heterogeneous, and non-secular fields may be applied to spin-lock and adiabatic passage methods as well as the described RF gradient sequences.

The broad acceptance of RF gradients as part of the NMR design tools has been slow since, to date, the only robust hardware has been to use the residual RF field inhomogeneity of an otherwise homogeneous RF coil. Advances in pin-diode switching and next generation probe technology will provide a platform for carrying out the methods introduced in the thesis, and will allow the selectivity and sensitivity advantage of RF gradients to be fully realized.

References

[1.1] A. Bax, P. G. De Jong, A. F. Mehlkopf and J. Smidt, Chem. Phy. Letters. Vol. **69**, Num. 3, 567, 1980

[1.2] P. Barker, R. Freeman, J. Magn. Reson., **64**, 224. 1985

[1.3] R. E. Hurd, J. Magn. Reson., **93**, 54. 1990

[1.4] D. Canet, D. Boudot, and J. Brondeau, J. Magn. Reson. **79**, 377. 1988

[1.5] D. Canet, J. Brondeau, E. Mischler, and F. Humbert, J. Magn. Reson. A, **105**, 239. 1993

[1.6] W. E. Maas, and D. G. Cory, J. Magn. Reson. A, **106**, 256. 1994

[1.7] W. E. Maas, F. H. Laukien, and D. G. Cory, J. Magn. Reson. A, **103**, 115. 1993

[1.8] D. G. Cory, F. H. Laukien, and W. E. Maas, Chem. Phys. Lett., **212**, 487. 1993

[1.9] P. Mutzenhardt, J. Brandeau, and D. Canet, J. Magn. Reson. A, **108**, 110. 1994

[1.10] C. J. R. Counsell, M. H. Levitt, and R. R. Ernst, J. Magn. Reson., **64**, 470. 1985

[1.11] J. Brondeau, D. Boudot, P. Mutzenhardt, and D. Canet, J. Magn. Reson., **100**, 611. 1992

[1.12] D. G. Cory, F. H. Laukien, and W. E. Maas, J. Magn. Reson. **105**, 223. 1993

[1.13] D. Canet, J. Mutzenhardt, and J. Brondeau, Molec. Phys., **84**, 597. 1995

[1.14] J. J. Titman, A. L. Davis, E. D. Laue, and J. Keeler, J. Magn. Reson., **89**, 176, 1990

[1.15] G. Estcourt, A. L. Davis, and J. Keeler, J. Magn. Reson., **96**, 191. 1992

[1.16] A. L. Davis, G. Estcourt, J. Keeler, E. D. Laue, and J. J. Titman, J. Magn. Reson. A, **105**, 167. 1993

[1.17] C. D. Eads, J. Magn. Reson. A, **107**, 109. 1994

[1.18] G. Otting, and K. Wuthrich, J. Magn. Reson., **76**, 569. 1988

[1.19] J-M. Nuzillard, G. Gasmi, and J.-M. Bernassau, J. Magn. Reson. a, **104**, 83. 1993

[1.20] W. E. Maas, and D. G. Cory, J. Magn. Reson. A, **112**, 229. 1995

[1.21] L. Mitschang, H. Ponstingl, D. Grindrod, and H. Sochkinat, J. Chem. Phys., **102**, 3089. 1995
[1.22] O.W. Sorensen, G. W. Eich, M. H. Levitt, G. Bodenhausen and R. R. Ernst, Progress in NMR Spectroscopy, **16**, 163. 1983
[2.1] G. Drobny, A. Pines, S. Sinton, D. Weitekamp, and D. Wemmer, Faraday Div. Chem. Soc. Symp. **13**, 49 (1979)
[5.1] Ernst, R. R., Bodenhausen, G., and Wokaun, A. 'Principles of Nuclear Magnetic Resonance in One and Two Dimensions', pp263. 1987, Clarendon Press.
[5.2] Ernst, R. R., Bodenhausen, G., and Wokaun, A. 'Principles of Nuclear Magnetic Resonance in One and Two Dimensions', pp340. 1987, Clarendon Press.
[5.3] Ernst, R. R., Bodenhausen, G., and Wokaun, A. 'Principles of Nuclear Magnetic Resonance in One and Two Dimensions', pp271. 1987, Clarendon Press.